Body mass, neuro-hormonal stress processing, and disease activity in lean to obese people with multiple sclerosis

Meyer-Arndt, L., Brasanac, J., Gamradt, S., Bellmann-Strobl, J., Maurer, L., Mai, K., Steward, T., Spranger, J., Schmitz-Hübsch, T., Paul, F., Gold, S.M. and Weygandt, M.

This is the final version of the accepted manuscript. The original article has been published in final edited form in:

Journal of Neurology
2024 APR; 271(04): 1584-1598
2023 NOV 23 (first published online: final publication)
Doi: 10.1007/s00415-023-12100-7

Publisher: Springer

Body mass, neuro-hormonal stress processing, and disease activity in lean to obese people with multiple sclerosis

Body mass, neuro-hormonal stress processing, and disease activity in lean to obese people with multiple sclerosis

Lil Meyer-Arndt[a,b,c,d,e], Jelena Brasanac[a,b,c,d,f], Stefanie Gamradt[f], Judith Bellmann-Strobl[a,b,c,e], Lukas Maurer[g,h,i,j], Knut Mai[g,j], Trevor Steward[k], Joachim Spranger[g,h,j], Tanja Schmitz-Hübsch[a,b,c,d], Friedemann Paul[a,b,c,d,e*], Stefan M. Gold[f,l,m*], Martin Weygandt[a,b,c,d,*,§]

[a] Experimental and Clinical Research Center, a cooperation between the Max Delbrück Center for Molecular Medicine in the Helmholtz Association and Charité Universitätsmedizin Berlin, Germany
[b] Charité – Universitätsmedizin Berlin, corporate member of Freie Universität Berlin and Humboldt-Universität zu Berlin, Experimental and Clinical Research Center, 13125 Berlin, Germany
[c] Max Delbrück Center for Molecular Medicine in the Helmholtz Association, 13125 Berlin, Germany
[d] Charité – Universitätsmedizin Berlin, corporate member of Freie Universität Berlin, Humboldt-Universität zu Berlin, and Berlin Institute of Health, NeuroCure Clinical Research Center, 10117 Berlin, Germany.
[e] Charité – Universitätsmed≥≥izin Berlin, corporate member of Freie Universität Berlin, Humboldt-Universität zu Berlin, and Berlin Institute of Health, Department of Neurology and Experimental Neurology, 10117 Berlin, Germany
[f] Charité – Universitätsmedizin Berlin, corporate member of Freie Universität Berlin, Humboldt-Universität zu Berlin, and Berlin Institute of Health, Department of Psychiatry and Psychotherapy, 12203 Berlin, Germany
[g] Charité – Universitätsmedizin Berlin, corporate member of Freie Universität Berlin, Humboldt-Universität zu Berlin, and Berlin Institute of Health, Department of Endocrinology and Metabolism, 10117 Berlin, Germany
[h] Charité – Universitätsmedizin Berlin, corporate member of Freie Universität Berlin, Humboldt-Universität zu Berlin, and Berlin Institute of Health, Max Rubner Center for Cardiovascular-Metabolic-Renal Research, 10117 Berlin, Germany
[i] Berlin Institute of Health, 10117 Berlin, Germany

[j] Charité – Universitätsmedizin Berlin, corporate member of Freie Universität Berlin, Humboldt-Universität zu Berlin, and Berlin Institute of Health, DZHK (German Centre for Cardiovascular Research), Partner Site Berlin, 13347 Berlin, Germany
[k] Melbourne School of Psychological Sciences, Faculty of Medicine, Dentistry and Health Sciences, University of Melbourne, Redmond Barry Building #817, Parkville, Victoria, 3010, Australia
[l] Charité – Universitätsmedizin Berlin, corporate member of Freie Universität Berlin, Humboldt-Universität zu Berlin, and Berlin Institute of Health, Department of Psychosomatic Medicine, 10117 Berlin, Germany
[m] Institute of Neuroimmunology and Multiple Sclerosis (INIMS), Center for Molecular Neurobiology Hamburg, Universitätsklinikum Hamburg-Eppendorf, 20251 Hamburg, Germany

Keywords: Multiple sclerosis, obesity, psychological stress, functional connectivity, glucocorticoid functioning

Acknowledgments and Funding: This work was supported by the German Research Foundation (WE 5967/2-1 and WE 5967/2-2 to MW, GO 1357/5-1 and GO 1357/5-2 to SMG, Exc 257 to FP). Our funding sources did not influence the study design, the collection, analysis and interpretation of data, the writing of the report or the decision to submit the article for publication.

*These authors contributed equally.

§Corresponding author. E-mail address: weygandtmartin@gmail.com

Abstract

Overweight and obesity can worsen disease activity in multiple sclerosis (MS). Although psychobiological stress processing is increasingly recognized as important obesity factor that is tightly connected to proinflammatory metabolic hormones and cytokines, its role for MS obesity remains unexplored.

Consequently, we investigated the interplay between body mass index (BMI), neural stress processing (functional connectivity, FC), and immuno-hormonal stress parameters (salivary cortisol and T cell glucocorticoid [GC] sensitivity) in 57 people with MS (6 obese, 19 over-, 28 normal-, and 4 underweight; 37 females, 46.4 ± 10.6 years) using an Arterial-Spin-Labeling MRI task comprising a rest and stress stage, along with quantitative PCR.

Our findings revealed significant positive connections between BMI and MS disease activity (i.e., higher BMI was accompanied by higher relapse rate). BMI was positively linked to right supramarginal gyrus and anterior insula FC during rest and negatively to right superior parietal lobule and cerebellum FC during stress. BMI showed associations with GC functioning, with higher BMI associated with lower $CD8^+$ FKBP4 expression and higher $CD8^+$ FKBP5 expression on T cells. Finally, the expression of $CD8^+$ FKBP4 positively correlated with the FC of right supramarginal gyrus and left superior parietal lobule during rest.

Overall, our study provides evidence that body mass is tied to neuro-hormonal stress processing in people with MS. The observed pattern of associations between BMI, neural networks, and GC functioning suggests partial overlap between neuro-hormonal and neural-body mass networks. Ultimately, the study underscores the clinical importance of understanding multi-system crosstalk in MS obesity.

1 Introduction

Overweight and obesity (subsequently summarized as "obesity") are linked to multiple sclerosis (MS) in several significant ways, as risk factors for developing MS during childhood and adolescence, particularly among women [1], and as modulatory factors aggravating clinical disability, neuroinflammation [2], and relapse rate [3] in people with MS (PwMS).

Research on obesity in established MS has focused on metabolic hormones and proinflammatory cytokines, which play crucial roles in the pathophysiology of both diseases [e.g., 4 – 6]. Specifically, endocrinological work highlights proinflammatory effects of adipocyte-released metabolic hormones such as leptin, a major regulator of energy homeostasis signaling satiety [5]. Leptin correlates positively with the body mass index (BMI; kg/m^2; [7]), upregulates proinflammatory cytokines, reduces regulatory T cells [7, 8] and increases with MS disability [9]. Immunological studies show that fat cells secrete high amounts of IL-6 and TNF-α [10]. Moreover, in PwMS, the counts of blood cell producing IL-2, IL-6, IL-15, IL-17, IFN-γ, and TNF-α increase as BMI increases [7], and obesity induces a shift towards proinflammatory T helper cells [11]. Together, these findings argue that a low-grade inflammation mediated by obesity is a key factor linking it to MS [3].

Neurocognitive food-intake mechanisms, such as incentive salience, goal-directed decision-making, and stress-processing, highly important contributors to obesity according to neuroscientific and endocrinological research (see e.g., [12] or our recent review [13]) that are able to overwrite hormonal (e.g., leptinergic) food-intake signals [14], were not yet studied in MS. Incentive salience, a process in the motivational mesolimbic reward system, can trigger food intake upon exposure to context stimuli of food consumption as these stimuli acquire reward-like properties through repeated coupling [12, 15]. The brain's goal-directed decision-making system can model action consequences and inhibit choices (e.g., eating palatable foods) predicted to yield unfavorable consequences [16, 17].

Stress will normally rapidly reduce hunger via corticotropin releasing hormone, but later increase appetite via cortisol release, which subsequently promotes a redistribution of white adipose tissue to the abdominal area [18]. By weakening the functional connectivity

3

(FC) between control areas and reward-prone regions (favoring unhealthy tasty foods) within the goal-directed decision-making system, stress reduces dietary control [19]. In the long run, individuals with obesity can learn that palatable food-intake reduces stress via reinforcement learning and thus establish stress-induced eating as a maladaptive coping mechanism [20]. Research has consistently found that people with obesity have a higher chance of gaining weight under stress [21] and are more likely to sustain weight reduction longer if they possess high stress tolerance [22]. Relatedly, obesity is associated with elevated glucocorticoid (GC) levels [23]. Abdominal obesity, in particular, has been linked to GC receptor (GR)-coding genes [24], and FK506-binding protein 5 (FKBP5, a co-chaperone regulating intracellular GR activity; [18]) is expressed differently in obesity [25]). Ultimately, stress is linked to abovementioned metabolic hormones and immunological parameters. For example, acute stress is accompanied by a decrease in serum leptin [26] and can heighten IFN-γ secretion in humans [27] and the number of IL-17 producing $CD4^+$ cells in mice [28].

Hence, there is substantial evidence emphasizing the importance of obesity for MS and the role of stress processing for obesity but these processes have not yet been investigated in MS. Thus, in this study, we conducted four main analyses in a cohort of 57 adults with MS featuring a wide range of different body mass indices. Firstly, inferred from previous research [e.g., 2, 3], we hypothesized that BMI is related to MS activity and severity measures and thus tested its associations with relapse rate, clinical disability, grey matter (GM) fraction and T2-weighted lesion load. Secondly, we used a widely established Arterial-Spin-Labeling (ASL) functional MRI (fMRI) stress task [e.g., 29 – 34] to test associations between BMI and FC among stress-reactive brain regions. Following [19], we hypothesized that FC during stress would correlate with BMI. Thirdly, we tested links between BMI and measures of GC functioning (i.e., salivary cortisol and T cell GC sensitivity) which were available for patient subsamples. Finally, we tested whether FC of BMI-related stress-reactive regions correlates with parameters of BMI-related T cell GC sensitivity to evaluate the overlap between neural-body mass and neuro-hormonal networks.

4

2 Methods

2.1 Participants

The study combines data from two study projects carried out by the Experimental and Clinical Research Center and the NeuroCure Clinical Research Center at Charité - Universitätsmedizin Berlin, which included a clinical and an MRI visit maximally two weeks apart. In particular, we pooled stress fMRI data collected in the first study project and evaluated in Weygandt et al. [33] and stress fMRI data collected in the second study project and analyzed in Brasanac et al. [29]. Please note, that stress fMRI data acquired in the first project were analyzed for non-body mass related purposes also in [31, 32, 35], those acquired in the second were additionally evaluated for non-body mass related purposes in [35]. Again, not related to body mass, data on GC functioning were also analyzed in [29]. Comparable inclusion criteria were applied across projects: Patients had to meet the 2010 McDonald criteria [36] for relapsing-remitting or secondary-progressive MS in the first project and criteria for relapsing-remitting in the second. Patients were required to receive a disease-modifying treatment (DMT) continuously for at least the last six (first project) or three (second project) months prior to study participation or no DMT in this period. They were only included if they were 18 years or older and when able to operate the task devices in an unrestricted fashion. Exclusion criteria comprised MRI contraindications, an additional neurologic disorder or acute MS relapse, steroid treatment in the four weeks prior to participation, and an insufficient anatomical image quality assessed visually by M.W. in both projects. Additionally, individuals were excluded in the first project if they confirmed the presence of a mental health diagnosis after being asked for such diagnoses (which included diagnoses of a depressive and an anxiety disorder) in a basic medical anamnesis conducted by a neurologist during the clinical visit appointment. In the second, individuals were excluded if a psychotherapist identified a mental health illness other than a depressive or anxiety disorder using the Mini-International Neuropsychiatric Interview [37]. Further, we excluded the data acquired in the first study project of those 16 patients who took part in both projects to guarantee that only one data set per individual was included. Specifically, in this step, the data acquired in the first project were excluded due to the slightly lower image

5

resolution of the T1-weighted scans acquired in the first compared to the second study project (see section 2.6 MRI acquisition below and the Supplement for information on MRI sequence parameters including their spatial resolution). From the pooled sample of 60 patients (20 first, 40 second project), we finally removed data from three patients with pronounced head motion during functional scans indicated by the Framewise Displacement metric as further quality assurance step (see Supplement for details). Consequently, data of 57 PwMS were analyzed. Please refer to Fig. 1 for an illustration of the patient selection procedure in terms of a flowchart. The projects were conducted in accordance with the Helsinki Declaration of 1975 and approved by the ethics committee of Charité – Universitätsmedizin Berlin (first project: EA1/182/10, amendment V; second: EA1/208/16). Written informed consent was obtained from all participants.

2.2 Clinical assessments

Neurological impairment was assessed at the clinical visit using the Expanded Disability Status Scale (EDSS; [38]). BMI was assessed directly after arrival in the imaging center with a calibrated scale (Kern, Balingen-Frommern, Baden-Württemberg, Germany) and a stadiometer (Seca, Hamburg, Hamburg, Germany). The Beck Depression Inventory (BDI)-II [39] was used in the first project for measuring depressive symptom severity, BDI-I [40] in the second. We combined the results from both measurements into a common metric using the algorithm of [41]. For more clinical measures assessed, refer to Weygandt et al. [42].

2.3 Diurnal salivary cortisol

During the clinical visit in study project two, the patients received instructions for collecting saliva at home. These instructions guided participants to measure their salivary cortisol levels both upon waking and after 9 p.m. on the two days preceding the MRI scan (i.e. four samples were acquired per patient in total). The samples were returned at the MRI visit and then centrifuged for 5 minutes at 1000 × g, aliquoted, and stored at -20 °C until analysis. Following the manufacturer's instructions, an ELISA (IBL, Germany) was used to determine the cortisol level. Salivary cortisol data for 34 PwMS were available. Based on the raw data,

6

we computed the average diurnal cortisol level and the hourly decline with linear regression and entered these parameters in main analysis 3.

2.4 Gene expression within the glucocorticoid pathway of T cells

In study project two, we measured the gene expression of four key components of GC signaling, FK506-binding protein 4 (FKBP4) and FKBP5, glucocorticoid-induced leucine zipper (GILZ), and the glucocorticoid receptor (GR), for $CD4^+$ and $CD8^+$ T cells. Acting as a co-chaperon, FKBP5 modifies the activity of the GR, the essential receptor for immunomodulation, and thereby modulates the stress response in the immune system [43]. FKBP5 is replaced by FKBP4 when GC binds to the GR, which initiates nuclear translocation and subsequent transcriptional activity. Lastly, GILZ is transcriptionally activated by GR and initiates the main anti-inflammatory GC effects, especially in T cells [44]. Using a real-time PCR system, complementary DNA was amplified to measure the expression of these four markers in the T cell subpopulations. The gene expression was then normalized to that of housekeeping genes by computing delta cycle threshold (ΔCT) values via subtracting the geometric mean of the CT values of the housekeeping genes from the mean CT values of the genes of interest. These markers were available for 37 PwMS. The Supplement provides further information, including specifics on the isolation of peripheral blood mononuclear cells, the sorting of $CD4^+$ and $CD8^+$ T cells, RNA isolation, cDNA synthesis, and real-time reverse transcription PCR.

2.5 fMRI stress paradigm

The paradigm included seven stages in the first project (1. Rating I, 2. Rest, 3. Rating II, 4. Stress, 5. Rating III, 6. Rest II, 7. Rating IV), while in project two, it comprised stages 1 to 5. In stage 4, the patients had to complete a series of mental mathematic tasks. Specifically, in substage 4a (“Evaluation”), we tested the participants’ mental arithmetic performance level and accordingly provided feedback in substage 4b (“Feedback”). A nine-point Likert scale (1 - "not at all" to 9 - "strongly") was used to measure perceived stress in the rating stages (2 min each). The second (8 min) and fourth (12 min) stages were used to collect ASL and heart

7

rate data (Supplement). In the present study, we used the data from stages 1 to 5. These stages are described in Fig. 2.

2.6 MRI acquisition

MRI acquisition took place between 3 and 7 p.m. to control for circadian variations. All MR images were acquired with the same 3 Tesla whole-body tomograph (Magnetom Trio, Siemens, Erlangen, Germany) and standard 12-channel head coil. A pseudo-continuous ASL sequence [30] was used to acquire fMRI scans during the stress paradigm. Field maps were acquired for distortion correction of ASL scans. Anatomical images were acquired with T1-weighted and T2-weighted sequences. See also Supplement.

2.7 MRI preprocessing

2.7.1 Anatomical scans

A lesion mapping was carried out by raters from the group of F.P. based on T2-weighted images. The standard preprocessing conducted with SPM12 (Wellcome Trust Centre for Neuroimaging, Institute of Neurology, University College London, London, UK, http://www.fil.ion.ucl.ac.uk/spm) included a spatial mapping of participants' T2-weighted to T1-weighted scans and a combined spatial normalization and segmentation of T1-weighted scans. During normalization, the T1-weighted images were co-registered to the Montreal Neurological Institute (MNI; [45]) standard space. Moreover, a computation of tissue-specific (i.e., GM, white matter [WM], and cerebrospinal fluid [CSF]) group masks and of the patients' whole-brain GM fraction and lesion volume was performed based on tissue voxel maps resulting from the segmentation (Supplement).

2.7.2 Functional scans

Preprocessing of ASL scans was performed with (toolboxes for) SPM12 (Supplement). It included head motion correction, B0 distortion correction, co-registration to the raw T1-

8

weighted images and, subsequently, co-registration to the MNI standard space (voxel resolution $3 \cdot 3 \cdot 3$ mm^3). Mapping to MNI space was performed by applying the co-registration parameters computed for the T1-weighted anatomical scans described in the above section. Finally, the ASL scans were smoothed in the spatial domain using a three-dimensional gaussian kernel (8 mm full width at half maximum). Afterwards, we extracted regional Cerebral Blood Flow (rCBF; ml/100g/min) timeseries voxel-by-voxel for all participants and conditions separately. Data from the (final) eight minutes of both conditions were used for all subsequent procedures. We concentrated on the last eight minutes of the stress condition as this period was consistently included in the "Feedback" stress substage 4b across all participants.

2.8 Regional neural stress reactivity and functional connectivity within patients

To provide the source data for main analysis 2, we computed parameters of (i) regional neural stress reactivity (indicated by stress vs. rest *activity* differences of regions included in the Neuromorphometrics brain atlas; http://Neuromorphometrics.com) and of (ii) pair-of-region-wise FC within patients. For (i), we first generated an rCBF timeseries for each individual, condition, and GM region in the atlas. These timeseries were calculated by averaging the timeseries of individual voxels located in a single atlas region that had non-zero rCBF and were covered by the GM group mask. The individual voxels' timeseries were corrected for the participant's head motion and global WM and CSF timeseries signals beforehand. A region was excluded from all analyses if it did not contain a single voxel in one or more participants meeting these requirements. 119 out of 122 atlas regions were included. By contrasting the regions' averaged stress vs. rest activity timeseries, regional activity differences were calculated as stress-reactivity markers with linear regression for each PwMS. The resulting regression coefficients were used to evaluate regional stress reactivity on the group-level in main analysis 2. For (ii), we computed the (Fisher Z-transformed) correlation coefficient for the averaged regional rCBF timeseries of all pairs of areas as FC parameter per patient and condition. FC between regions showing significant stress reactivity was used for testing group-level BMI-FC relations in analysis 2. See the Supplement for details. It's worth noting that just like resting-state FC, task-based FC (in this case, during

9

stress) can be computed as the correlation between the timeseries of pairs of brain regions [e.g., 13, 46). FC was chosen as neural parameter due to the pivotal role of regional interplay for obesity [e.g., 13, 19, 47]. ASL was selected because it is a quantitative MRI method for measuring rCBF that is increasingly used in neuroscientific FC studies (see e.g., the review of Chen et al. [48]) due to its higher robustness to slow signal noise relative to that of the alternative blood-oxygenation-level-dependent (BOLD) fMRI technique [30].

2.9 Statistical analysis

2.9.1 Main analysis 1: BMI and MS activity and severity

To test associations between BMI and disease activity as well as severity in MS, we conducted four robust regression analyses in which we regressed the four dependent variables (DVs) annualized relapse rate (for disease activity), clinical disability, whole-brain T2-weighted lesion load, and GM fraction (for disease severity) individually on BMI (the covariate of interest; CI). Sex, age, study project, depressive symptom severity, disease duration, presence of progressive MS and disease modifying treatment were modeled as covariates of no interest (CNI). Additionally, the three DV not tested for in each DV-specific analysis were also modeled as CNI (e.g., when annualized relapse rate served as DV, clinical disability, whole-brain T2-weighted lesion load, and GM fraction also served as CNI). Significance was evaluated with permutation testing in undirected tests. Here, as well as in all other permutation analyses, 10,000 permutations of the CI vector were conducted. A family-wise-error (FWE)-corrected significance threshold of $\alpha_{FWE} = 0.05$ corresponding to $0.05 / 4 = 0.0125$ on a single test-level was applied. We report Cohen's [49] effect size measure f^2 ($f^2 \geq 0.02$ weak, $f^2 \geq 0.15$ medium, and $f^2 \geq 0.25$ strong effect).

2.9.2 Main analysis 2: BMI and functional connectivity of stress-reactive brain regions

For testing associations between BMI and FC, we determined stress-reactive regions on the group-level in a first step and then related the stress stage and resting stage FC between stress-reactive regions to BMI across patients in a second. Specifically, using the regression coefficients described in section 2.8 as dependent variables, we employed robust linear regression to determine if there were differences in the regions' activity during stress vs. rest

10

across patients. CNI were all DV and CNI evaluated in main analysis 1. Additionally, cognitive task load (i.e., the average inter-trial period in the final eight minutes of the stress stage) and time-to-feedback (i.e., the duration of substage 4b) were modeled as stress task-specific CNI. Modeling cognitive task load is essential to control for putative effects of task demands and mental arithmetic performance. Significance was evaluated with permutation testing. An FWE-corrected significance threshold of α_{FWE} = 0.05 was applied in undirected tests corresponding to 0.05 divided by 119 (number of brain regions in the analysis) or $4.2 \cdot 10^{-4}$ respectively on a single test level. An analysis of stress reactivity in terms of psychological stress (i.e., stress ratings) and of peripheral stress reactivity (i.e., heart rate) can be found in the Supplement (supplementary analysis 1). After stress-reactive regions were identified, we regressed the FC of each pair of stress-reactive regions on BMI using robust linear regression. This was done separately for resting and stress stage FC. CNI were identical to those used for the identification of stress-reactivity. Permutation testing was employed to test for significance in undirected pair-of-region-wise tests. Given that 17 regions turned out to be stress-reactive (see Results, main analysis 2) and thus $17 \cdot [17 - 1] / 2 = 136$ tests were conducted per condition, we applied an α_{FWE} of 0.05 equal to $0.05 / (17 \cdot [17 - 1] / 2) = 3.68 \cdot 10^{-4}$ on a single test level. Notably, we conducted an analysis in the Supplement that regressed the neural stress-reactivity parameters (i.e., the abovementioned coefficients) of stress-reactive regions on participants' BMI (supplementary analysis 2) to help evaluate the relative suitability of FC for BMI prediction performed in main analysis 2.

2.9.3 Main analysis 3: BMI and glucocorticoid functioning

We tested associations between BMI and the average diurnal cortisol level and its hourly decline (α_{FWE} = 0.05 equal to 0.05 / 2 on a single test level). Moreover, we tested potential links between BMI and the gene expression of FKBP4, FKBP5, GILZ and GR in $CD4^+$ and $CD8^+$ T cells (α_{FWE} = 0.05 equal to 0.05 / 8 on a single test level). For cortisol and T cell GC sensitivity analyses, CNI included all DV and CNI of main analysis 1.

2.9.4 Main analysis 4: BMI-related glucocorticoid and neural processing markers

11

To investigate whether stress and BMI-related brain regions are also related to BMI-related measures of T cell GC functioning, we tested associations between resting stage FC of stress-reactive brain regions whose resting stage FC was associated with BMI (see Results, main analysis 2) on one hand and BMI-related GC sensitivity T cell markers (see Results, main analysis 3) on the other. The same was done for FC of the respective regions involved during stress. The regression and inference methods (including the CNI) were identical to Analysis 2. GC parameters served as CI, FC as DV. Given that the number of tests in each of the two families of tests (as in main analysis 2 one for FC during rest, one for FC during stress) was $2 \cdot (2 \cdot 16 - 1) = 62$, $\alpha_{FWE} = 0.05$ equaled to $\alpha = 0.05 / 62 = 8.1 \cdot 10^{-4}$ on a single test level. For an exact explanation of this number, see Supplement. At this point, we would like to mention that we report the impact of patients' sex on all DV tested across main analyses 1 - 4 in terms of the test statistics determined by the robust regression models in these analyses for the CNI sex. Moreover, we conduct complementary categorial analyses (i.e., Analyses of Covariance; ANCOVA) in supplementary analysis 4 testing differences between body mass groups (i.e., obesity [BMI ≥ 30], overweight [25 ≥ BMI > 30], etc.) in the DV tested in the main analyses with linear regression based on the continuous BMI variable.

12

3 Results

3.1 Clinical and demographic participant characteristics

Six of the 57 PwMS were obese (BMI ≥ 30), 19 overweight (25 ≥ BMI > 30), 28 normal weight (18.5 ≥ BMI > 25), and four underweight (BMI < 18.5). Five patients were treated with teriflunomide, ten with dimethyl fumarate, nine with fingolimod, eight with glatiramer acetate, and ten with β-interferons (see Tab. 1 for further details).

3.2 Main analysis 1: BMI and multiple sclerosis severity

Out of the four activity/severity parameters tested, the association between BMI and annualized relapse rate was significant ($t = 3.23$, $p = 0.003 = p_{FWE} = 0.012$, $f^2 = 0.22$). The links to the other parameters were not (EDSS: $t = -0.88$, $p = 0.378 = p_{FWE} > 0.999$, $f^2 = 0.01$; lesion load: $t = 0.26$, $p = 0.792$, $= p_{FWE} > 0.999$, $f^2 = -0.00$; GM fraction: $t = 0.24$, $p = 0.812 = p_{FWE} > 0.999$, $f^2 = -0.01$; see Fig. 3). Please note that the latter small negative f^2 values result from specifics of f^2 and the use of robust coefficients of determination R^2_{full} and R^2_{base} for its computation. For further details, refer to the Supplement.

3.3 Main analysis 2: BMI and functional connectivity

Seventeen widely distributed brain regions showed significant stress–rest activity differences and were thus considered as stress-reactive (Fig. 4a). BMI was significantly linked to resting stage FC between right anterior insula and right supramarginal gyrus ($t = 4.02$, $p = 2.5 \cdot 10^{-4}$, $p_{FWE} = 0.034$, $f^2 = 0.51$). For stress stage FC, we found a significant association between right cerebellum exterior and right superior parietal lobule ($t = -3.67$, $p = 3.3 \cdot 10^{-4}$, $p_{FWE} = 0.045$, $f^2 = 0.30$). See Fig. 4b – d.

13

3.4 Main analysis 3: BMI and glucocorticoid functioning

The associations between BMI and salivary cortisol failed to reach significance (diurnal average: $t = 1.48$, $p = 0.139 = p_{FWE} = 0.278$, $f^2 = 0.01$; hourly decline: $t = -2.28$, $p = 0.031 = p_{FWE} = 0.062$, $f^2 = 0.01$). Out of the four GC sensitivity markers assessed per T cell subpopulation, a significant link to BMI was obtained for FKBP4 ($t = -2.96$, $p = 0.003 = p_{FWE} = 0.024$, $f^2 = 0.13$) and FKBP5 ($t = 1.83$, $p = 0.003 = p_{FWE} = 0.024$, $f^2 = 0.38$) expression of $CD8^+$ cells. Please note that the comparably small t of 1.83 given $p = 0.003$ in this association was caused by a single data point whose effect on p was, however, well mitigated by the combined application of robust regression and permutation testing. See Fig. 5.

3.5 Main analysis 4: BMI-related glucocorticoid and neural processing markers

Testing associations between gene expression of the BMI-correlated T cell GC sensitivity markers (see Results, main analysis 3) on one hand and FC of stress-reactive brain regions whose mutual FC was associated with BMI (see Results, main analysis 2) on the other showed a significant positive link between FKBP4 expression in $CD8^+$ T cells and resting stage FC between left superior parietal lobule and right supramarginal gyrus ($t = 5.30$, $p = 7.0 \cdot 10^{-5} = p_{FWE} = 4.5 \cdot 10^{-3}$, $f^2 = 1.47$; Fig. 6).

14

4 Discussion

Even though obesity is linked to MS in several important ways, essential neurocognitive obesity mechanisms, including psychobiological stress, have never been investigated in people with MS. We employed an fMRI stress task to study whether neural stress processing is related to body mass in 57 underweight to obese PwMS. Additionally, we tested whether BMI is related to salivary cortisol and T cell GC sensitivity in patient subsamples and whether BMI-related GC sensitivity and neural processing parameters are linked.

Four main analyses were conducted. The first tested basic associations between BMI and MS activity and severity parameters. This showed a significant association with relapse rate which is consistent with Escobar et al. [3]. A related supplementary analysis (i.e., supplementary analysis 3) focusing on the link between sex and the DV tested in main analyses 1 – 4 revealed a significant relationship between sex and GM fraction (however, at a liberal $\alpha_{FWE} = 0.1$ level only). Male patients tended to have a lower GM fraction than females. This result is consistent with a study by Voskuhl and colleagues [50], which reported higher regional GM atrophy in male patients, suggesting that male sex may be a risk factor for more severe MS progression.

We next tested associations between BMI and FC of stress-reactive regions in main analysis 2. The first part of the analysis, which evaluated regional stress reactivity, identified 17 regions (Fig. 4a) typically involved in stress processing (e.g., compare [30]), which (together with findings of supplementary analysis 1 on psychophysiological stress responses) underlines the ability of this task to induce stress. The second part showed that, among all pairs of these 17 areas, BMI was linked to FC of right anterior insula and right supramarginal gyrus during rest, which is highly compatible with findings reported in the literature. In particular, insula is a key region in a network underlying incentive salience [51], a comparably simple mechanism initiating food seeking and consumption after exposure to food cues (such as visual food percepts) as these cues were coupled to reward (i.e., food intake) in the learning history of an individual via Pavlovian conditioning. Consequently, the

15

cues become predictive of reward and acquire similar motivational properties as food itself after they were coupled repeatedly to the food [12, 15]. Consistent with this function, insula shows enhanced activity to food cues [52] and its responses to food cues correlate positively with BMI [53]. Furthermore, insula and supramarginal gyrus are both parts of the salience resting-state network [47], whose function is to identify the most relevant stimuli for guiding subsequent behavior [54]. Consistently, heightened activity of this network was also reported for obese vs. non-obese people [47]. Thus, consistent with the fact that heightened incentive salience was found to be one of if not the most important driver(s) of BMI in non-MS studies [13] and the involvement of anterior insula and supramarginal gyrus in (neural networks underlying) incentive salience of food stimuli, the link between BMI and these regions' FC found here is compatible with a positive link of incentive salience of food stimuli and BMI also in PwMS.

During the stress stage, we observed a significant negative relationship between BMI and FC of right superior parietal lobule and cerebellum exterior. This finding can be explained by integrating findings on neural processes of dietary self-control and stress. In detail, van der Laan et al. [55] found that superior parietal cortex is an area involved in dietary self-control by showing that when healthy persons choose low-caloric, non-tasty but healthy foods in a food-choice task (i.e., when exerting self-control) activity in this area increases when compared to choosing unhealthy but tasty foods (i.e., when exerting no self-control). Furthermore, cerebellum is a key region underlying the generation of stressful and affectively negative states (also showing neural emotion processing alterations in obese persons [56]) with a high stress hormone receptor density and strongly connected to other stress regions [57]. Thus, when considering that stress (e.g., induced by cerebellar activity) promotes unhealthy food choices by reducing FC between control and reward-prone regions in the brain's decision-making system (favoring unhealthy tasty foods; see [19]), one can inversely assume that self-control increases and BMI thus decrease if a stress-generating region (here: cerebellum) adapts its activity to that of a control region (here: superior parietal lobule) with higher adaptation being reflected by higher FC between these areas. With other words, the observed negative relation between BMI and FC between right superior parietal lobule and cerebellum exterior during stress presumably indicates an inverse relationship between neural self-control and BMI.

16

Furthermore, the presence of BMI–FC relationships in main analysis 2 but the absence of such relationships between BMI and the activity of individual stress-reactive brain regions in supplementary analysis 2, suggests that employing FC to study associations between BMI and neural processes was an appropriate choice.

In main analysis 3, we first tested associations between BMI and the average and hourly decline in diurnal salivary cortisol, which, however, failed to reveal significant results on an FWE-corrected level. This was different for T cell GC sensitivity: Among the eight markers tested (expression of FKBP4 and 5, GILZ and GR on $CD4^+$ and $CD8^+$ T cells), associations between BMI and FKBP4 as well as FKBP5 on $CD8^+$ T cells were significant. This finding is consistent with results showing altered GC sensitivity in obese people without MS in [24] and [25] and underlines the relation of GC functioning and body weight in MS.

Finally, in main analysis 4, we aimed at evaluating whether FC of stress-reactive brain regions whose FC correlates with BMI also correlates with BMI-related parameters of GC functioning in order to determine the overlap between neural-body mass and neural-immuno-hormonal networks. We demonstrated a significant link of CD8+ FKBP4 gene expression and resting state FC between left superior parietal lobule and right supramarginal gyrus. Although evaluating patients with a different disease, our findings are in line with a study of Koh and colleagues [58], who investigated associations between resting state brain activity and immune functioning in somatoform disorder and found a hypoperfusion in inferior parietal lobule and supramarginal gyrus in patients with strong (i.e., lower lymphocyte proliferative responses to phytohemagglutinin) vs. weak immune suppression. Compatible with our interpretation of the association between resting state FC of superior parietal lobule and right supramarginal gyrus and CD8+ FKBP4 gene expression, the authors concluded that the parietal regions they identified are involved in modulation of immune functions. In both cases, this interpretation is supported by the fact that parietal cortex is strongly connected to insular cortex [59], which is not only a key region for mediation of incentive salience [51] but again critical for measuring and modulating immune functions [60]. Thus, although BMI-related GC functioning was not related to resting state FC of the same pair of stress-reactive seed-target regions that was linked to BMI (i.e., FC between right anterior insula and right supramarginal gyrus), the pair related to GC functioning again

17

comprised right supramarginal gyrus, which at least indicates a partial overlap among brain-BMI and brain-immuno-hormonal networks.

An aspect worth mentioning is that although the patterning of results obtained for testing effects of interest via categorial variables/the body mass groups in supplementary analysis 4 and via the continuous variables in the main analyses was quite comparable, not a single ANCOVA evaluating categorial variables was significant for $\alpha_{FWE} = 0.05$. This may initially appear surprising, but it becomes understandable when considering how categorial body mass groups are defined: by thresholding the existing continuous BMI measure (i.e., BMI ≥ 30: obesity; 25 ≥ BMI > 30: overweight, etc.). This procedure, however, is intentionally discarding meaningful information as 54 different BMI values (two persons had a BMI of 19.9 and three of 23.2) are mapped to only four different body mass classes and it creates somewhat arbitrary distinctions (e.g., a person having a BMI of 29.9 is treated identical to one with a BMI of 25 but different to one of BMI 30). Consequently, such categorial analyses have lower statistical power compared to those based on the original continuous BMI variable [61]. Finally, in the context of our study with its small to moderate group size, this disadvantageous feature by far outweighs the increased modeling flexibility provided by categorial analyses (potentially indicated by the strongest, though still non-significant, association between body mass and FC during stress, showing an inverse U-shape for right frontal operculum and right supplementary cortex; Figure S4b).

Another aspect worth discussing is the use of ASL for analyzing FC as BOLD fMRI is still considered the most widely used FC technique [48]. However, two factors indicate that ASL is highly suitable for studying FC. First, the number of clinical ASL FC studies has been rising recently (e.g., [62 – 65]) and already the review of Chen and colleagues from 2015 [48] summarizes six ASL FC studies. This shows that the technique is used in a substantial body of FC research. Second, studies evaluating signal detection properties of ASL FC found that it reliably identifies established resting-state networks such as the salience and default-mode networks [66]. Maybe more important, however, is the fact that ASL is much less affected by slow signal artifacts than BOLD [30]. Thus, a slow signal, if observed, can be retained due to its attribution to the underlying experimental condition, in this case stress, which is known to be a slow phenomenon [67]. For BOLD, in contrast, slow signal variations can not only be

18

induced by the experimental condition, but also by noise. Thus, removing such signals becomes a necessity but it may not only remove artifacts but simultaneously the experimentally induced signal (co)variation.

Additionally, it is important that, while the sample size was not predefined based on a sample size calculation, the present work evaluates a large number of patients compared to similar MS fMRI studies (i.e., according to the review by Rocca et al. [68], it evaluates a larger number of patients than 88% of all MS fMRI studies employing cognitive tasks).

A limitation of the study is that anxiety was only measured in a categorial/dichotomous fashion (i.e., whether an anxiety disorder was present or not). Future studies should additionally characterize and model this parameter in terms of continuous questionnaire measures reflecting anxiety severity. Furthermore, although we accounted for a variety of nuisance factors through statistical modeling (e.g., sex, age, study project, depressive symptom severity, disease duration, presence of progressive MS, DMT application, annualized relapse rate, clinical disability, T2-weighted lesion load, GM fraction, cognitive task load, and time-to-feedback served as CNI in the key main analysis 2), it should be noted that the patients included exhibited comparable heterogeneity in terms of clinical and demographic variables. Finally, another limitation is that we did not standardize eating behavior on the day before the MRI scan which should be considered in future studies.

5 Conclusions

Our study shows that stress-related neural as well as immune-hormonal markers are linked to BMI in PwMS across the body mass spectrum. Further, associations observed between stress-reactive neural networks linked to BMI and those linked to GC functioning suggest that neural-body mass and neuro-hormonal networks partially overlap.

19

6 Statements and declarations

Competing interests

The authors declare no conflicts of interest.

Contribution statement

Lil Meyer-Arndt: Data analysis, investigation, writing, reviewing, editing.

Jelena Brasanac: Data analysis, data curation, reviewing, editing.

Stefanie Gamradt: Data analysis, reviewing, editing.

Judith Bellmann-Strobl: Project administration, reviewing.

Lukas Maurer: Data curation, reviewing.

Knut Mai: Resources, reviewing.

Trevor Steward: Reviewing, editing.

Joachim Spranger: Resources, reviewing.

Tanja-Schmitz Hübsch: Project administration, reviewing.

Friedemann Paul: Resources, project administration, reviewing, editing.

Stefan Gold: Reviewing, editing.

Martin Weygandt: Resources, conceptualization, data curation, data analysis, visualization, writing, reviewing, editing.

20

References

1. Gianfrancesco MA, Barcellos LF. Obesity and Multiple Sclerosis Susceptibility: A Review. Neurol Neuromedicine. 2016; 1(7): 1-5.

2. Bassi MS, Iezzi E, Buttari F, Gilio L, Simonelli I, Carbone F, et al. Obesity worsens central inflammation and disability in multiple sclerosis. Multiple Sclerosis Journal 2019.

3. Escobar JM, Cortese M, Edan G, Freedman MS, Hartung H-P, Montalban X, Sandbrink R, Radü E-W, Barkhof F, Wicklein E-M, Kappos L, Ascherio A, Munger KL. Body Mass Index as a predictior of MS activity and progression among participants in BENEFIT. Mult Scler. 2022; 28(8):1277-1285.

4. Vreeken D, Seidel F, de La Roij G, Vening W, den Hengst WA, Verschuren L, Özsezen S, Kessels RPC, Duering M, Mutsaerts HJMM, Kleemann R, Wiesmann M, Hazebroek EJ, Kiliaan AJ. Impact of White Adipose Tissue on Brain Structure, Perfusion, and Cognitive Function in Patients With Severe Obesity: The BARICO Study. Neurology. 2023 Feb 14;100(7):e703-e718.

5. Schreiner TG, Genes TM. Obesity and Multiple Sclerosis—A Multifaceted Association. J Clin Med. 2021; 10, 2689.

6. Guerrero-Garcia JJ, Carrera-Quintanar L, Lopez-Roa RI, Marquez-Aguirre AL, Rojas-Mayorquin AE, Ortuno-Sahagun D. Multiple Sclerosis and Obesity: Possible Roles of Adipokines. Mediators Inflamm. 2016; 2016:4036232.

7. Marrodan M, Farez MF, Balbuena Aguirre ME, Correale J. Obesity and the risk of Multiple Sclerosis. The role of Leptin. Ann Clin Transl Neurol. 2021; 8: 406-424.

8. Matarese G, Biagio Carrieri P, La Cava A, Perna F, Sanna V, De Rosa V. Leptin increase in multiple sclerosis associates with reduced number of CD4(+)CD25+ regulatory T cells. Proc Natl Acad Sci USA. 2005; 102, 5150-55.

21

9. Fahmi RM, Kamel AE, Elsayed DA, Zidan AA, Sarhan NT. Serum levels of leptin and adiponectin in patients with multiple sclerosis. Egypt J Neurol Psychiatry Neurosurg. 2021; 57, 114.

10. Asghar A, Sheikh N. Role of immune cells in obesity induced low grade inflammation and insulin resistance. Cell Immunol. 2017; 315: 18-26.

11. Balasa R, Maier S, Barcutean L, Stoian A, Motataianu A. The direct deleterious effect of Th17 cells in the nervous system compartment in multiple sclerosis and experimental autoimmune encephalomyelitis: one possible link between neuroinflammation and neurodegeneration. Rev Romana Med Laborator. 2020, 28.

12. Volkow ND, Wise RA, Baler R. The dopamine motive system: implications for drug and food addiction. Nat Rev Neurosci. 2017;18(12):741-52.

13. Kozarzewski K, Maurer, Mähler A, Spranger J, Weygandt M. Computational approaches to predicting treatment response to obesity using neuroimaging. Reviews in Endocrine and Metabolic Disorders. 2022; 23: 773-805.

14. Egecioglu E, Skibicka KP, Hansson C, Alvarez-Crespo M, Friberg PA, Jerlhag E, Engel JA, Dickson SL. Hedonic and incentive signals for body weight control. Rev Endocr Metab Disord. 2011 Sep;12(3):141-51.

15. Robbins TW, Ersche KD, Everitt BJ. Drug addiction and the memory systems of the brain. Ann N Y Acad Sci. 2008; 1141:1-21. doi:10.1196/annals.1441.020.

16. Weygandt M, Spranger J, Leupelt V, Maurer L, Bobbert T, Mai K. Interactions between neural decision-making circuits predict long-term dietary treatment success in obesity. NeuroImage. 2019; 84: 520 – 534.

17. Rangel A. Regulation of dietary choice by the decision-making circuitry. Nat Neurosci. 2013; 16: 1717-24.

18. Van der Valk ES, Savas M, van Rossum EFC. Stress and Obesity: Are There More Susceptible Individuals? Curr Obes Rep. 2018; 7: 193–203.

19. Maier SU, Makwana AB, Hare TA. Acute Stress Impairs Self-Control in Goal-Directed Choice by Altering Multiple Functional Connections within the Brain's Decision Circuits. Neuron. 2015, 87, 621–631.

20. Guerrero-Hreins E, Goldstone AP, Brown RM, Sumithran P. The therapeutic potential of GLP-1 analogues for stress-related eating and role of GLP-1 in stress, emotion and mood: a review. Prog Neuropsychopharmacol Biol Psychiatry. 2021;110:110303.

21. Block JP, He Y, Zaslavsky AM, Ding L, Ayanian JZ. Psychosocial stress and change in weight among US adults. Am J Epidemiol. 2009; 170, 181–192.

22. Thom G, Dombrowski SU, Brosnahan N, Algindan YY. The role of appetite-related hormones, adaptive thermogenesis, perceived hunger and stress in long-term weight-loss maintenance: a mixed-methods study. Eur J Clin Nutr. 2020; 74 (4), 622–632.

23. Wester VL, Staufenbiel SM, Veldhorst MAB, Visser JA, Manenschijn L, Koper JW. Long-term cortisol levels measured in scalp hair of obese patients. Obesity (Silver Spring). 2014; 22(9):1956–8.

24. Rosmond R, Chagnon YC, Holm G, Chagnon M, Perusse L, Lindell K, et al. A Glucocorticoid Receptor Gene Marker Is Associated with Abdominal Obesity, Leptin, and Dysregulation of the Hypothalamic- Pituitary-Adrenal Axis. Obes Res. 2000; 8:211-8.

25. Menke A, Kloiber S, Best J, Rex-Haffner M, Uhr M, Holsboer F, Binder EB. GR-mediated FKBP5 RNA induction differentially influenced by weight in major depression and healthy controls. Pharmacopsychiatry. 2013; 46 - A15. DOI: 10.1055/s-0033-1353276

26. Maes M, Song C, Lin A, De Jongh R, Van Gastel A, Kenis G, Bosmans E, De Meester I, Benoy I, Neels H, Demedts P, Janca A, Scharpé S, Smith RS. The effects of psychological stress on humans: increased production of pro-inflammatory cytokines and a Th1-like response in stress-induced anxiety. Cytokine. 1998;10(4):313-8.

27. Bouillon-Minois J-B, Trousselard M, Thivel D, Benson AC, Schmidt J, Moustafa F, Bouvier D, Dutheil F. Leptin as a Biomarker of Stress: A Systematic Review and Meta-Analysis. Nutrients. 2021 Sep 24;13(10):3350.

23

28. Ambrée O, Ruland C, Zwanzger P, Klotz L, Baune BT, Arolt V, Scheu S, Alferink J. Social Defeat Modulates T Helper Cell Percentages in Stress Susceptible and Resilient Mice. Int J Mol Sci. 2019 Jul 17;20(14):3512.

29. Brasanac J, Hetzer S, Asseyer S, Kuchling J, Bellmann-Strobl J, Ritter K, Gamradt S, Scheel M, Haynes JD, Brandt AU, Paul F, Gold SM, Weygandt M. Central stress processing, T cell responsivity to stress hormones, and disease severity in multiple sclerosis. Brain Commun. 2022; 4: fcac086.

30. Wang J, Rao H, Wetmore GS, Furlan PM, Korczykowski M, Dinges DF, Detre JA. Perfusion functional MRI reveals cerebral blood flow pattern under psychological stress. Proc Natl Acad Sci U S A. 2005; 102:17804-9.

31. Meyer-Arndt L, Schmitz-Hübsch T, Bellmann-Strobl J, Brandt AU, Haynes JD, Gold SM, Paul F, Weygandt M. Neural processes of psychological stress and relaxation predict the future evolution of quality of life in multiple sclerosis. Front Neurol. 2021; 12:753107.

32. Meyer-Arndt L, Hetzer S, Asseyer S, Bellmann-Strobl J, Scheel M, Stellmann J-P, Heesen C, Engel AK, Brandt AU, Haynes J-D, Paul F, Gold SM, Weygandt M. Blunted neural and psychological stress processing predicts future grey matter atrophy in multiple sclerosis. Neurobiol Stress. 2020; 13:100244.

33. Weygandt M Meyer-Arndt L Behrens J, Wakonig K, Bellmann-Strobl J, Ritter K, Scheel M, Brandt AU, Labadie C, Hetzer S, Gold SM, Paul F, Haynes JD. Stress-induced brain activity, brain atrophy, and clinical disability in Multiple Sclerosis. Proc Natl Acad Sci U S A. 2016; 113: 13444-13449.

34. Wang JJ, Korczykowski M, Rao H, Fan Y, Pluta J, Gur RC, McEwen BS, Detre JA. Gender difference in neural response to psychological stress. Soc Cogn Aff Neurosci. 2007; 2: 227-239.

35. Schulz MA, Hetzer S, Eitel F, Asseyer S, Meyer-Arndt L, Schmitz-Hübsch T, Bellmann-Strobl J, Cole JH, Gold SM, Paul F, Ritter K, Weygandt M. Similar neural pathways link psychological stress and brain-age in health and multiple sclerosis. iScience. 2023; 26:107679. doi: 10.1016/j.isci.2023.107679.

24

36. Polman CH, Reingold SC, Banwell B, Clanet M, Cohen JA, Filippi M. Diagnostic criteria for multiple sclerosis: 2010 revisions to the McDonald criteria. Ann Neurol. 2011; 69 (2): 292 - 302.
37. Sheehan DV, Lecrubier C, Sheehan KH, Amorim P, Janavs J, Weiller E, Hergueta T, Baker R, Dunbar GC. Mini-International Neuropsychiatric Interview (M.I.N.I.): the development and validation of a structured diagnostic psychiatric interview for DSM-IV and ICD-10. J Clin Psychiatry. 1998; 59; 20:22-30.
38. Kurtzke JF. Rating neurologic impairment in multiple sclerosis: An expanded disability status scale (EDSS). Neurology. 1983; 33:1444-52.
39. Hautzinger M, Keller F and Kuhner C. BDI-II: Beck-Depressions-Inventar (Revision. 2nd Edition). Frankfurt: Pearson Assessment, 2009.
40. Beck AT, Ward CH, Mendelson M, Mock J, Erbaugh J. An inventory for measuring depression. Arch Gen Psychiatry. 1961; 4:561-71.
41. Wahl I, Löwe B, Bjorner JB, Fischer F, Langs G, Voderholzerg U. Standardization of depression measurement: a common metric was developed for 11 self-report depression measures. J Clin Epidemiol. 2014; 67 (2014) 73e86.
42. Weygandt M, Wakonig K, Behrens J, Meyer-Arndt L, Söder E, Brandt AU, Bellmann-Strobl J, Ruprecht R, Gold SM, Haynes J-D, Paul F. Brain activity, regional grey matter loss, and decision-making in Multiple Sclerosis. Mult Scler. 2018; 24: 1163 – 1173.
43. Zannas AS, Wiechmann T, Gassen NC, Binder EB. Gene-Stress-Epigenetic Regulation of FKBP5: Clinical and Translational Implications. Neuropsychopharmacology. 2016; 41:261-274.
44. Cannarile L, Delfino DV, Adorisio S, Riccardi C, Ayroldi E. Implicating the Role of GILZ in Glucocorticoid Modulation of T-Cell Activation. Front Immunol. 2019;10:1823.
45. Tzourio-Mazoyer, N, Landeau B, Papathanassiou D, Crivello F, Etard O, Delcroix N. Automated anatomical labeling of activations in SPM using a macroscopic anatomical parcellation of the MNI MRI single-subject brain. Neuroimage. 2002; 15 (1), 273-89.

46. Paolini BM, Laurienti PJ, Simpson SL, Burdette JH, Lyday RG, Rejeski WJ. Global integration of the hot-state brain network of appetite predicts short term weight loss in older adult. Front Aging Neurosci. 2015; 7: 70.
47. García-García I, Jurado MÁ, Garolera M, Segura B, Sala-Llonch R, Marqués-Iturria I. Alterations of the salience network in obesity: A resting-state fMRI study. Hum Brain Mapp. 2013;34: 2786–2797.
48. Chen JJ, Jann K, Wang DJJ. Characterizing Resting-State Brain Function Using Arterial Spin Labeling. Brain Connectivity. 2015; 5: 527 - 542.
49. Cohen J. Statistical Power Analysis for the Behavioral Sciences. 1988; 2nd ed., Lawrence Erlbaum Associates: Hillsdale.
50. Voskuhl RR, Patel K, Paul F, Gold SM, Scheel M, Kuchling J, Cooper G, Asseyer S, Chien C, Brandt AU, Meyer CE, MacKenzie-Graham A. Sex differences in brain atrophy in multiple sclerosis. Biol Sex Differ. 2020 Aug 28;11(1):49. doi: 10.1186/s13293-020-00326-3.
51. Naqvi NH, Gaznick N, Tranel D, Bechara A. The insula: a critical neural substrate for craving and drug seeking under conflict and risk. Ann N Y Acad Sci. 2014; 1316: 53-70.
52. Jastreboff AM, Sinha R, Lacadie C, Small DM, Sherwin RS, Potenza MS. Neural Correlates of Stress- and Food Cue-Induced Food Craving in Obesity. Association with insulin levels. Diabetes Care. 2013; 36:394-402.
53. Rothemund Y, Preuschhof C, Bohner G, Bauknecht HC, Klingebiel R, Flor H, Klapp BF. Differential activation of the dorsal striatum by high-calorie visual food stimuli in obese individuals. Neuroimage. 2007; 37: 410-21. doi: 10.1016/j.neuroimage.2007.05.008.
54. Menon V, Uddin LQ. Saliency, switching, attention and control: a network model of insula function. Brain Struct Funct. 2010; 214(5-6): 655-667.
55. Van der Laan LN, de Ridder DTD, Viergever MA, Smeets PAM. Activation in inhibitory brain regions during food choice correlates with temptation strength and self-regulatory success in weight-concerned women. Front Neurosci. 2014; 8; 308.
56. Steward T, Picó-Pérez M, Mata F, Martínez-Zalacaín I, Cano M, Contreras-Rodríguez O, et al. Emotion Regulation and Excess Weight: Impaired Affective Processing Characterized

26

by Dysfunctional Insula Activation and Connectivity. PLoS One. 2016. 11:e0152150. doi: 10.1371/journal.pone.0152150.

57. Moreno-Rius J. The cerebellum under stress. Front Neuroendocrinol. 2019; 54: 100774. doi:10.1016/j.yfrne.2019.100774

58. Koh KB, Sohn SH, Kang JI, Lee YJ, Lee JD. Relationship between neural activity and immunity in patients with undifferentiated somatoform disorder. Psychiatry Res. 2012;202(3):252-6.

59. Fermin ASR, Friston K, Yamasaki S. An insula hierarchical network architecture for active interoceptive inference. R Soc Open Sci. 2022;9(6):220226.

60. Koren T, Yifa R, Amer M, Krot M, Boshnak N et al. Insular cortex neurons encode and retrieve specific immune responses. Cell. 2021;184(24):5902-5915.e17.

61. Lazic SE. Why we should use simpler models if the data allow this: relevance for ANOVA designs in experimental biology. BMC Physiol 8, 16 (2008).

62. Galazzo IB, Storti SF, Barnes A, De Blasi B, De Vita E, Koepp M. Arterial Spin Labeling Reveals Disrupted Brain Networks and Functional Connectivity in Drug-Resistant Temporal Epilepsy. Front Neuroinform. 2019; 12:101.

63. Boissoneault J, Letzen J, Lai S, O'Shea A, Craggs J, Robinson M, Staud R. Abnormal Resting State Functional Connectivity In Patients with Chronic Fatigue Syndrome: An Arterial Spin-Labeling fMRI Study. Magn Reson Imaging. 2016; 34(4): 603-608.

64. Liu Y, Li B, Feng N, Pu H, Zhang X, Lu H, Yin H. Perfusion Deficits and Functional Connectivity Alterations in Memory-Related Regions of Patients with Post-Traumatic Stress Disorder. PLoS ONE. 2016; 11(5): e0156016.

65. Fernandez-Seara MA, Mengual E, Vidorreta M, Castellanos G Irigoyen J, Erro W, Pastor MA. Resting State Functional Connectivity of the Subthalamic Nucleus in Parkinson's Disease Assessed Using Arterial Spin-Labeled Perfusion fMRI. Hum Brain Mapp. 2015; 36:1937-1950.

66. Vallée C, Maurel P, Corouge I, Barillot C. Acquisition Duration in Resting-State Arterial Spin Labeling. How Long Is Enough? Front Neurosci. 2020; 14:598.

67. Kirschbaum C, Pirke KM, Hellhammer DH. The 'Trier Social Stress Test'-a tool for investigating psychobiological stress responses in a laboratory setting. Neuropsychobiology 1993; 28: 76 – 81.
68. Rocca AM, Schoonheim MM, Valsassina, Geurts JJG, Filippi M. Task- and resting state fMRi studies in multiple sclerosis: from regions to systems and time-varying analysis. Current status and future perspective. Neuroimage Clin. 2022; 35: 103076.

28

Table

Table 1. Demographic and clinical patient characteristics across all 57 patients and stratified by body mass groups. Please note that the parameters for the individual body mass classes are only depicted for illustrative purposes; the analyses conducted in the main analyses of this work were not conducted in a categorial fashion/by determining differences between body mass groups but rather by evaluating associations between continuous CI scores (e.g., the individuals' BMI) and DVs across all participants with linear regression. Please see the Discussion for an explanation of why the latter is a better choice in the context of this work. Abbreviations: ARR, annualized relapse rate; BDI, Beck Depression Inventory; DD, disease duration since first signs; DMT, disease modifying treatment; EDSS, Expanded Disability Status Scale; f., female; GMF, whole-brain grey matter fraction; m., male; MN, mean; PROG, presence of progressive MS; pts., points; rel., relapses; SD, standard deviation; T2LL, whole-brain T2-weighted lesion load; yr., year; yrs., years.

		All	Under-weight	Normal weight	Over-weight	Obese
BMI (m/kg^2)	MN SD	24.7 4.3	17.8 0.4	22.4 1.8	27.0 1.5	33.0 4.0
Sex (f./m.)	#	37 / 20	3 / 1	20 / 8	11 / 8	3 / 3
Age (yrs.)	MN SD	46.4 10.6	42.5 10.5	44.4 10.6	48.9 10.6	50.5 9.8
BDI (pts.)	MN SD	8.2 7.3	9.0 10.0	7.0 6.3	9.2 8.7	9.8 6.3
EDSS (pts.)	MD RG	2.5 0 - 6	2.5 2 – 5.5	2.5 0 - 6	3 0 – 5.5	3.25 1.5 - 6
DD (yrs.)	MN SD	12.8 8.8	15.0 7.3	12.1 7.2	14.2 11.6	10.2 6.6
ARR (rel./ yr)	MN SD	0.62 0.44	0.43 0.07	0.48 0.27	0.69 0.51	1.13 0.57
PROG (y/n)	#	7 / 50	1 / 3	2 / 26	3 / 16	1 / 5
T2LL (cm^3)	MN SD	13.9 19.9	24.3 36.9	15.7 22.7	11.2 12.6	7.3 9.8
GMF	MN SD	0.38 0.05	0.39 0.03	0.38 0.05	0.39 0.06	0.37 0.04
DMT (y/n)	#	42 / 15	3 / 1	19 / 9	15 / 4	5 / 1

29

DMT (type)	#	8 glatiramer acetate, 9 fingolimod, 10 dimethyl fumarate, 10 interferon β, 5 teriflunomide, 15 none	2 dimethyl fumarate, 1 interferon β, 1 none	2 glatiramer acetate, 2 fingolimod, 5 dimethyl fumarate, 7 interferon β, 3 teriflunomide, 9 none	5 glatiramer acetate, 4 fingolimod, 3 dimethyl fumarate, 2 interferon β, 1 teriflunomide, 4 none	1 glatiramer acetate, 3 fingolimod, 1 teriflunomide, 1 none

30

Figure captions

Figure 1. Participant selection procedure. For details, see text.

Figure 2. fMRI Stress paradigm. The paradigm was divided into five stages. There were two parts to the stress stage: 4a ("Evaluation") and 4b ("Feedback"). Participants completed subtraction tasks across a number of trials in the Evaluation substage (4a). Within each task, the patients had to choose the correct solution for equations of the form "operand X minus operand Y" from a list of four possible solutions displayed on a screen with an MRI-compatible response box as quickly as they could. The start value of X was 43521 across all participants. In each of the trials in 4a (and 4b), operand Y was chosen at random (range: 1 – 99). In study project one, the duration of 4a was 4 minutes or shorter if a participant solved ten tasks correctly earlier. 4a had a fixed duration of 4 min in study project two. To account for this difference, we modelled the duration of 4a as CNI "time-to-feedback" in all regression analyses modeling stress fMRI data and evaluated only the rCBF data (and heart rate, cognitive task load or mental arithmetic performance data respectively) collected in the last 8 minutes of stage 4b. The time allotted in 4a to complete a task was 8 seconds. When the participant selected the correct response for a task, X was set to this correct response score in the following task. If the response was inaccurate or too slow, X stayed unchanged. 4a was followed immediately by 4b. 4b was different from 4a in three ways. First, each task included feedback (i.e., German school grades ranging from "1 - very good" to "5 - insufficient"). The difference between the participant's fastest accurate response in 4a and the response time of a specific trial in 4b was used to select the feedback or school grade respectively. Feedback for incorrect or tardy responses was always "5 - insufficient." In this instance, second, X was reset to 43521. Thirdly, according to the participant's performance, the time for response selection was adjusted. Beginning with at 8 seconds at the start of 4b, this time was decreased by 10% for correct responses and increased by 10% for incorrect or very sluggish answers. This flexible procedure was used to make sure that every participant continuously performed at their highest level possible and that performance was therefore comparable to other participants in terms of an individual performance norm.

Figure 3. Associations between BMI and multiple sclerosis activity and severity. The scatter graphs illustrate the associations found in analysis 1 for BMI and the four MS severity markers. To facilitate a more comfortable interpretation of body mass in these and all other scatter graphs, the dot colors highlight BMI-based body mass classes, with red dots corresponding to obese PwMS ($kg/m^2 \geq 30$), pink to overweight PwMS ($25 \geq kg/m^2 > 30$), light blue to normal weight PwMS ($18.5 \geq kg/m^2 > 25$) and darker blue dots finally represent underweight patients ($kg/m^2 < 18.5$). Again, we would like to mention, however, that these body mass classes (i.e., categorial representations of body mass) are only depicted for illustrative purposes. The regression models evaluated in this and all other main analyses included continuous CI (here: BMI scores) for reasons delineated in the Discussion; complementary categorial analyses are presented in the Supplement (due to their disadvantages also delineated in the Discussion).

31

Figure 4. BMI and functional connectivity of stress-reactive brain regions. 4a shows the 17 stress- reactive brain areas (i.e., with significant activity differences between the rest and stress stage) identified. The bar graph on the left depicts the t-statistics obtained for the stress – rest contrast for significant regions sorted by their coarse anatomical location. The two graphs in the middle/right of 4a correspond to surface renderings of regional stress reactivity. The heatmaps in 4b depict associations between BMI and FC of pairs of stress-sensitive regions separately for FC during the rest and the stress stage. The left scatter graph in 4c illustrates the association between the pair of regions with resting-stage BMI associations significant according to a threshold corrected for multiple comparison ($\alpha_{FWE} = 0.05$; right anterior insula to right supramarginal gyrus). The scatter graph on the right does so for the pair with a significant BMI to stress-stage FC association (right cerebellum exterior to right superior parietal lobule). Finally, 4d depicts the median coordinates of and illustrative connections between these regions.

Figure 5. Associations between BMI and parameters of glucocorticoid functioning. The graphs in 5a show associations between BMI and the average diurnal salivary cortisol level on the left and between BMI and hourly decline in diurnal cortisol on the right. 5b depicts the associations between BMI and the gene expression of four GC signaling-related markers in $CD4^+$ and $CD8^+$ T cells. In all graphs, the DV depicted on the y-axis is corrected for the respective CNI. Abbreviations: ΔCT: delta cycle threshold gene expression values; FKBP4, FK506-binding protein 4; FKBP5, FK506-binding protein 5, GILZ, glucocorticoid-induced leucine zipper; GR, glucocorticoid receptor.

Figure 6. Links between BMI-related glucocorticoid and neural processing markers. The upper heatmap in 6a shows associations between BMI-related T cell GC sensitivity markers (i.e., expression of FKBP4 and FKBP5 in $CD8^+$ T cells) and resting-state FC of the two brain regions whose mutual FC during rest was linked to BMI in analysis 2. The lower heatmap depicts the same for stress-stage FC. Across individual analyses (62 for rest, 62 for stress), the association between resting-state FC of left superior parietal lobule and right supramarginal gyrus with expression of FKBP4 in $CD8^+$ T cells was significant on an FWE-corrected significance level which is thus depicted in 6b. Finally, 6c illustrates the median coordinates of these two brain regions and their spatial connection.

32

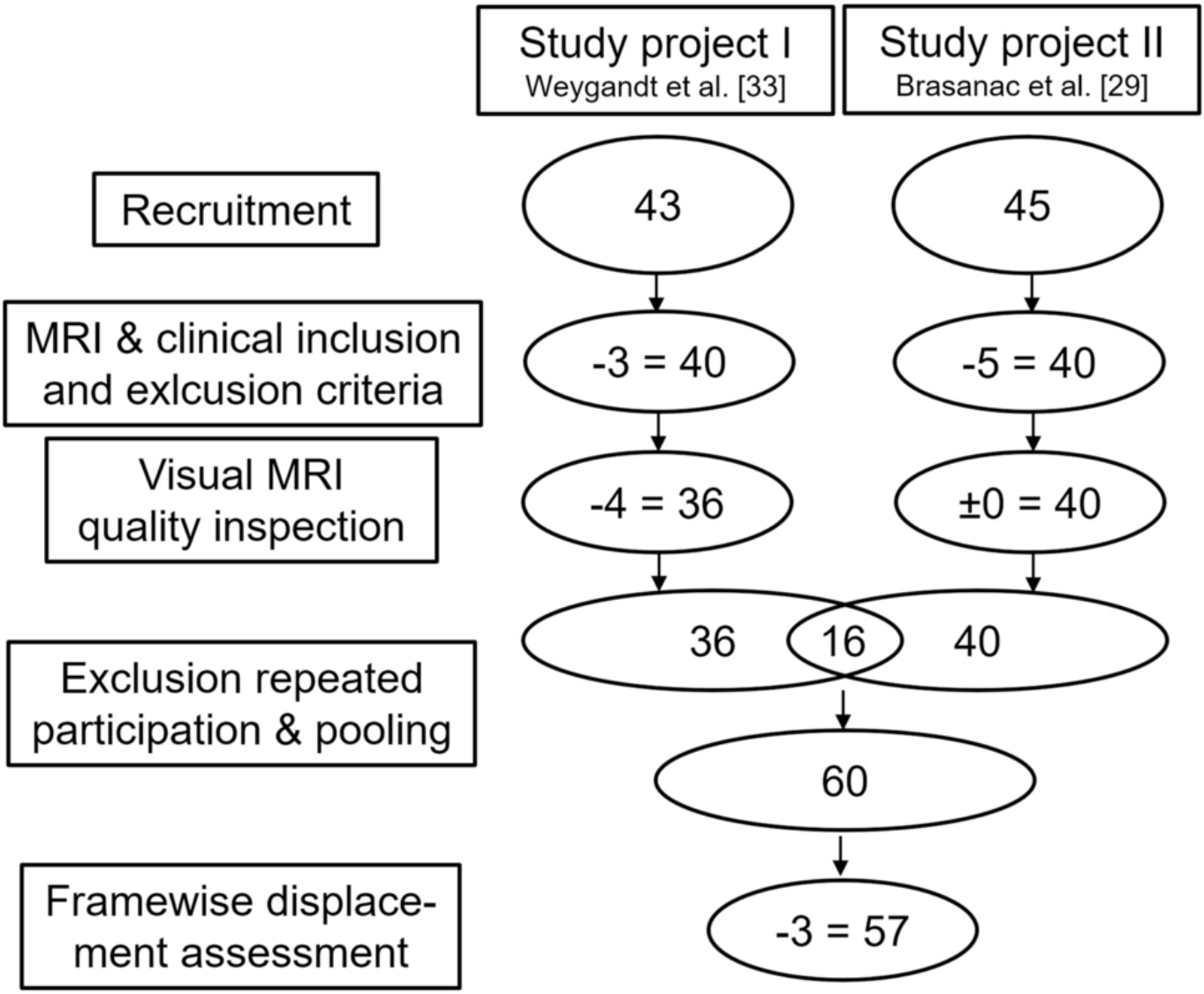
Study project I
Weygandt et al. [33]
Study project II
Brasanac et al. [29]
Recruitment
43
45
MRI & clinical inclusion and exlcusion criteria
-3 = 40
-5 = 40
Visual MRI quality inspection
-4 = 36
±0 = 40
36
16
40
Exclusion repeated participation & pooling
60
Framewise displace-ment assessment
-3 = 57

33

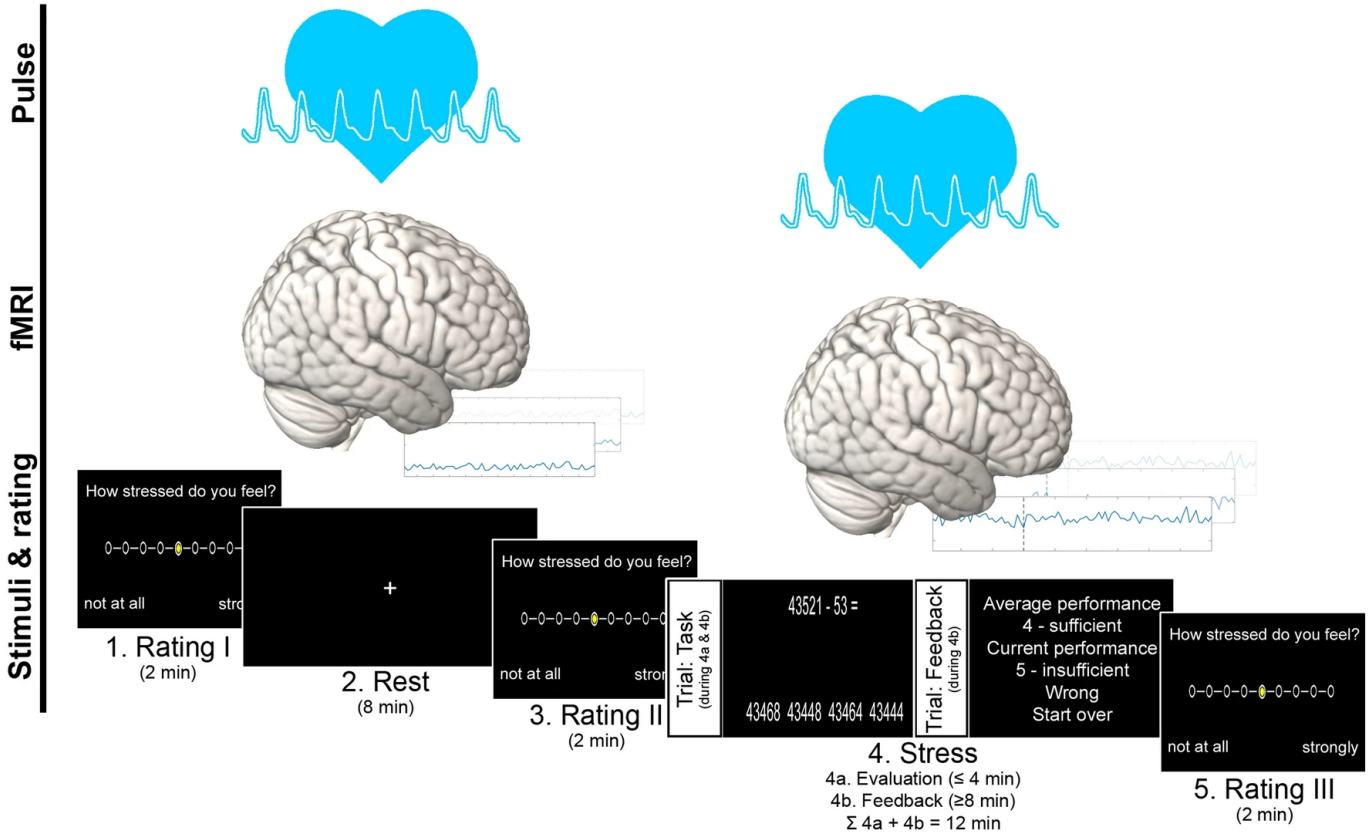
Pulse
fMRI
Stimuli & rating
How stressed do you feel?
not at all
1. Rating I
(2 min)
+
2. Rest
(8 min)
How stressed do you feel?
not at all
3. Rating II
(2 min)
Trial: Task
(during 4a & 4b)
43521 - 53 =
43468 43448 43464 43444
Trial: Feedback
(during 4b)
Average performance
4 - sufficient
Current performance
5 - insufficient
Wrong
Start over
4. Stress
4a. Evaluation (≤ 4 min)
4b. Feedback (≥8 min)
Σ 4a + 4b = 12 min
How stressed do you feel?
not at all
strongly
5. Rating III
(2 min)

34

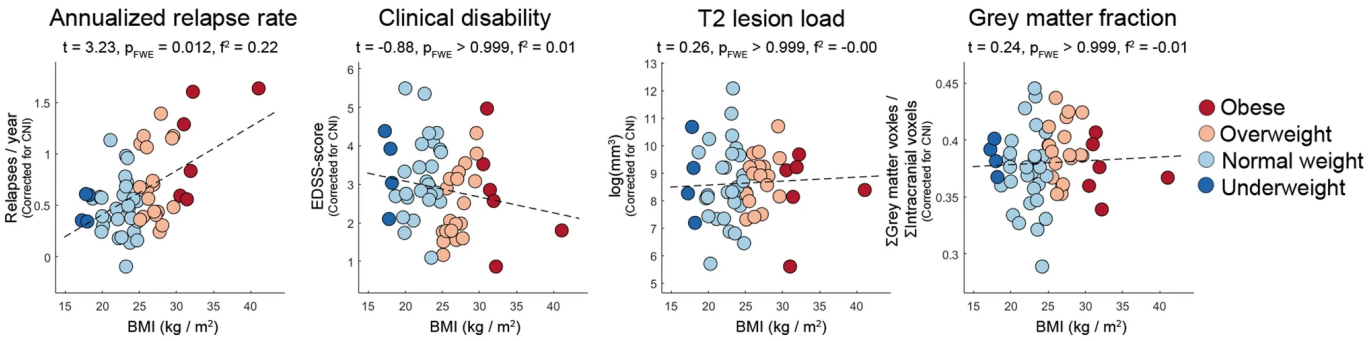

35

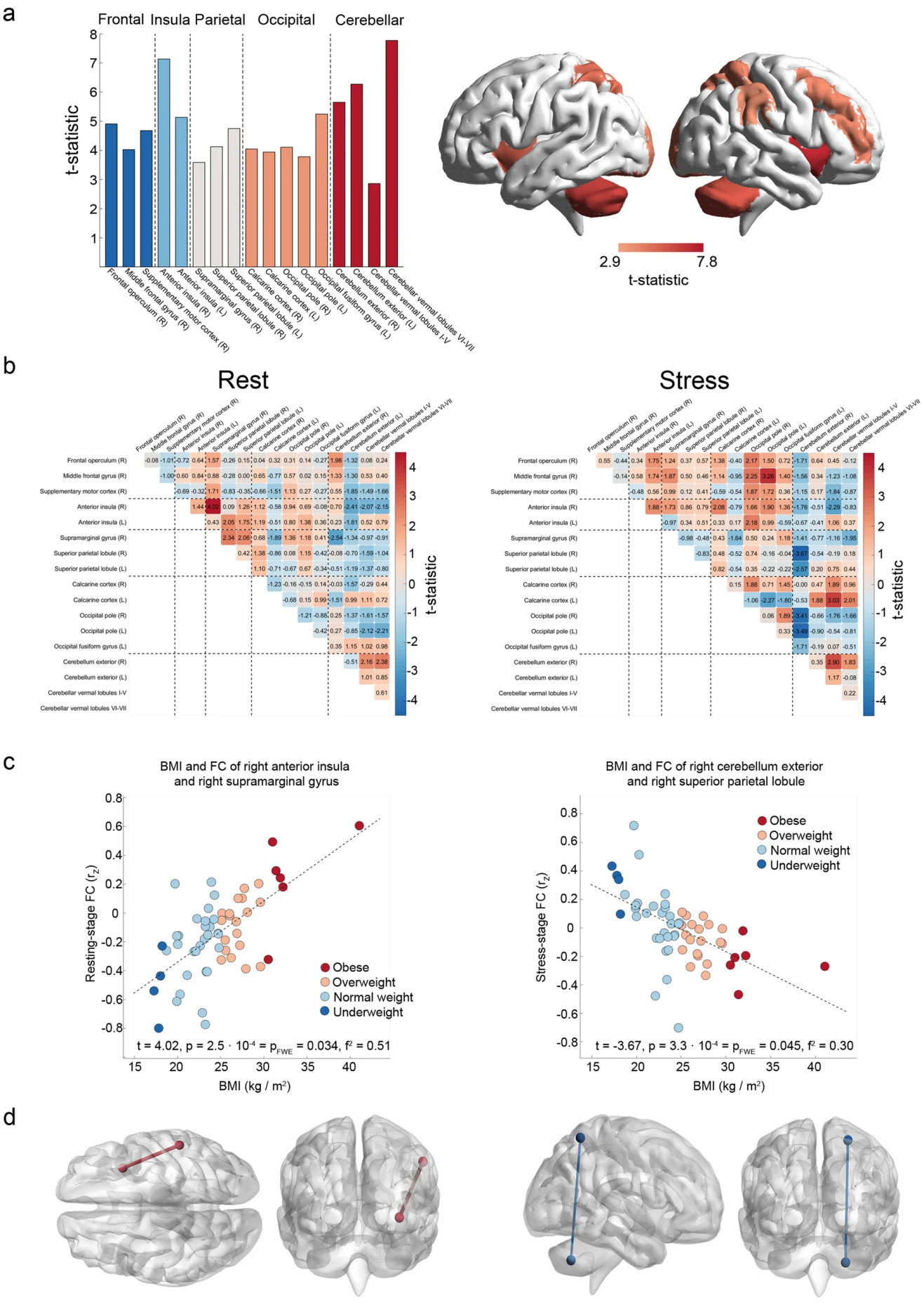
a
Frontal
Insula
Parietal
Occipital
Cerebellar
t-statistic
Frontal operculum (R)
Middle frontal gyrus (R)
Supplementary motor cortex (R)
Anterior insula (R)
Anterior insula (L)
Supramarginal gyrus (R)
Superior parietal lobule (R)
Superior parietal lobule (L)
Calcarine cortex (R)
Calcarine cortex (L)
Occipital pole (R)
Occipital pole (L)
Occipital fusiform gyrus (L)
Cerebellum exterior (R)
Cerebellum exterior (L)
Cerebellar vermal lobules I-V
Cerebellar vermal lobules VI-VII
2.9
7.8
t-statistic
b
Rest
Stress
t-statistic
c
BMI and FC of right anterior insula
and right supramarginal gyrus
Resting-stage FC (rz)
BMI (kg / m2)
Obese
Overweight
Normal weight
Underweight
t = 4.02, p = 2.5 · 10-4 = pFWE = 0.034, f2 = 0.51
BMI and FC of right cerebellum exterior
and right superior parietal lobule
Stress-stage FC (rz)
BMI (kg / m2)
Obese
Overweight
Normal weight
Underweight
t = -3.67, p = 3.3 · 10-4 = pFWE = 0.045, f2 = 0.30
d

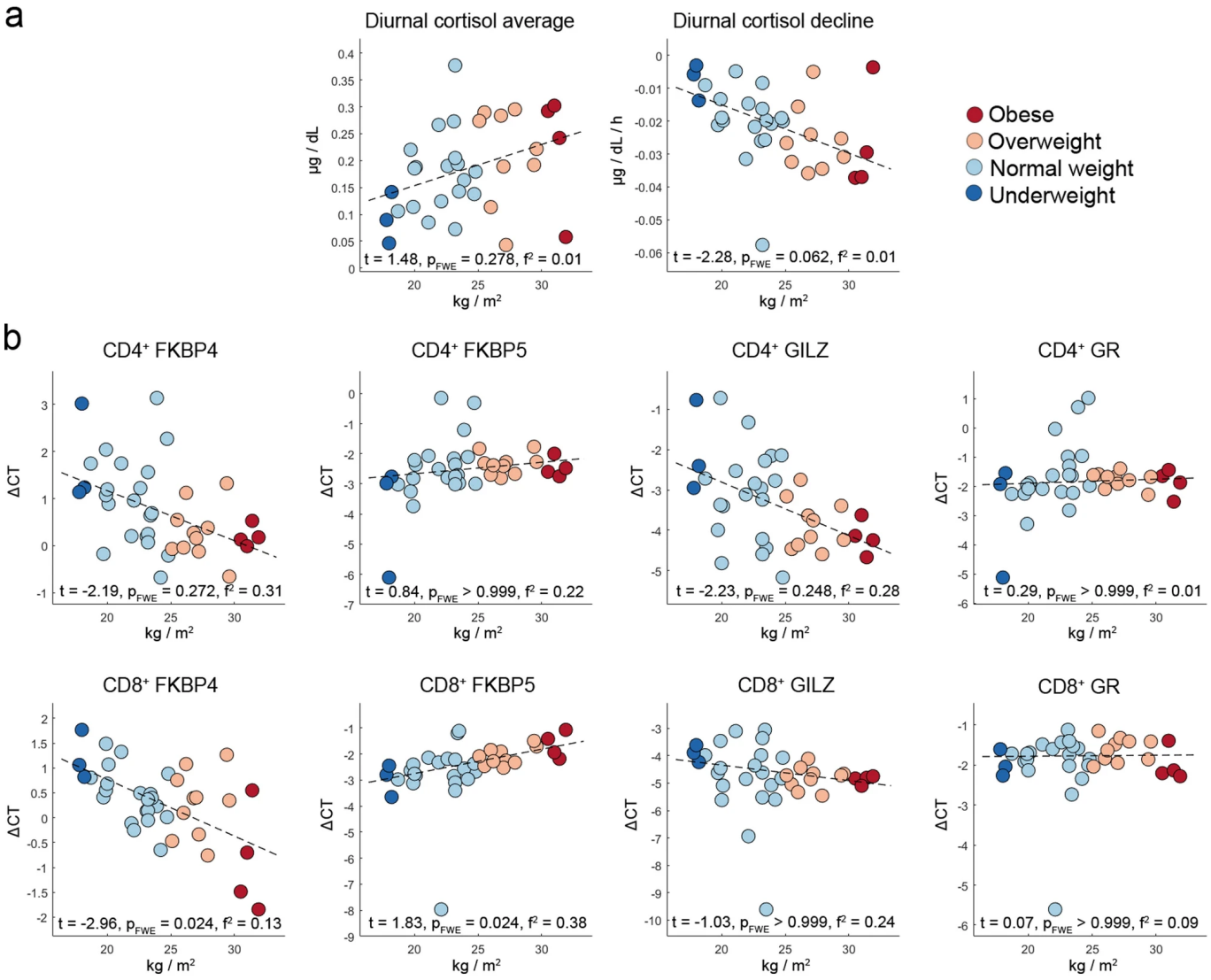
a
Diurnal cortisol average
µg / dL
t = 1.48, p_FWE = 0.278, f² = 0.01
kg / m²
Diurnal cortisol decline
µg / dL / h
t = -2.28, p_FWE = 0.062, f² = 0.01
kg / m²
Obese
Overweight
Normal weight
Underweight
b
CD4⁺ FKBP4
ΔCT
t = -2.19, p_FWE = 0.272, f² = 0.31
kg / m²
CD4⁺ FKBP5
t = 0.84, p_FWE > 0.999, f² = 0.22
CD4⁺ GILZ
t = -2.23, p_FWE = 0.248, f² = 0.28
CD4⁺ GR
t = 0.29, p_FWE > 0.999, f² = 0.01
CD8⁺ FKBP4
t = -2.96, p_FWE = 0.024, f² = 0.13
CD8⁺ FKBP5
t = 1.83, p_FWE = 0.024, f² = 0.38
CD8⁺ GILZ
t = -1.03, p_FWE > 0.999, f² = 0.24
CD8⁺ GR
t = 0.07, p_FWE > 0.999, f² = 0.09

37

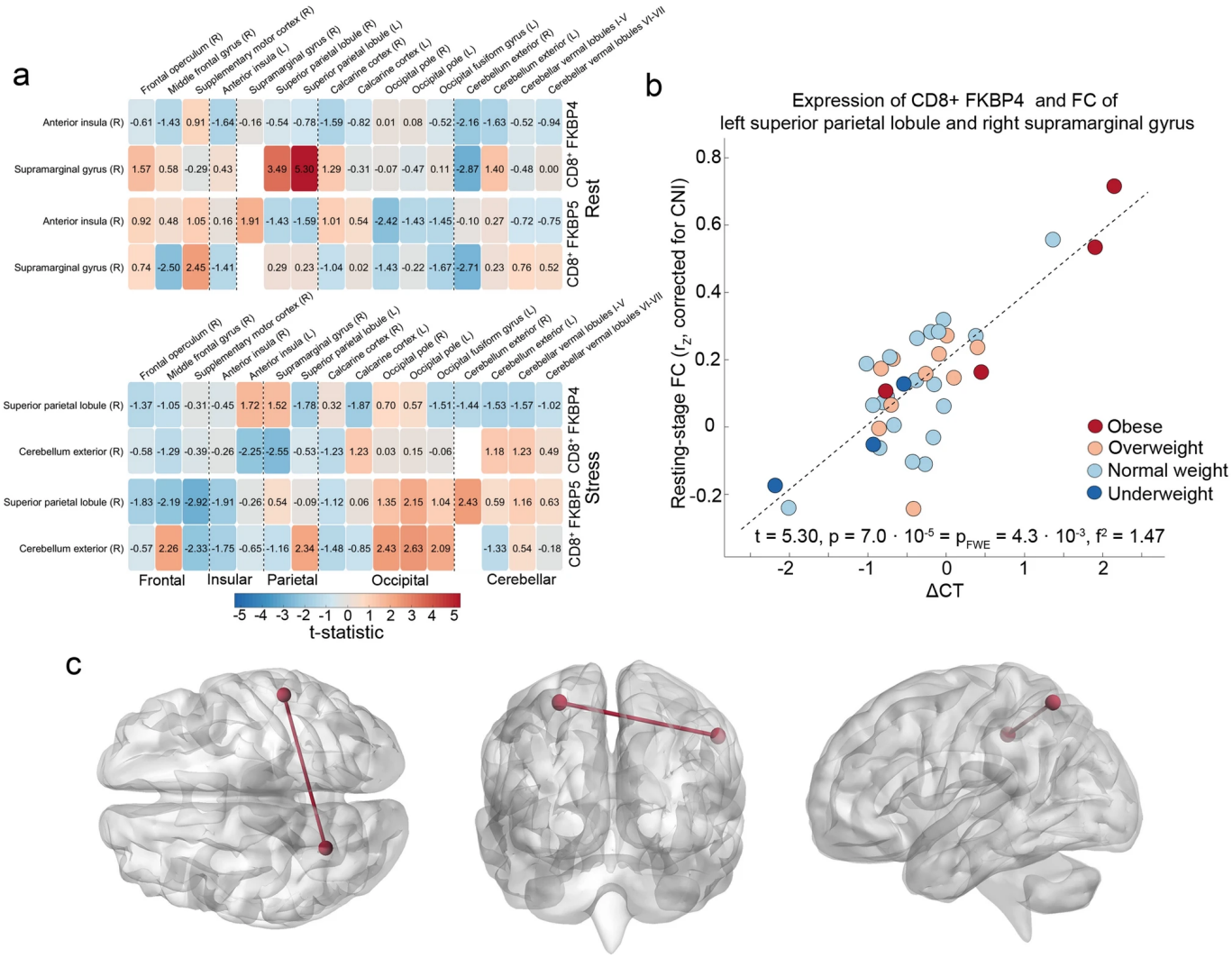

38

Body mass, neuro-hormonal stress processing, and disease activity in lean to obese people with multiple sclerosis

Lil Meyer-Arndt[a,b,c,d,e], Jelena Brasanac[a,b,c,d,f], Stefanie Gamradt[f], Judith Bellmann-Strobl[a,b,c,e], Lukas Maurer[g,h,i,j], Knut Mai[g,j], Trevor Steward[k], Joachim Spranger[g,h,j], Tanja Schmitz-Hübsch[a,b,c,d], Friedemann Paul[a,b,c,d,e*], Stefan M. Gold[f,l,m*], Martin Weygandt[a,b,c,d,*,§]

[a] Experimental and Clinical Research Center, a cooperation between the Max Delbrück Center for Molecular Medicine in the Helmholtz Association and Charité Universitätsmedizin Berlin, Germany
[b] Charité – Universitätsmedizin Berlin, corporate member of Freie Universität Berlin and Humboldt-Universität zu Berlin, Experimental and Clinical Research Center, 13125 Berlin, Germany
[c] Max Delbrück Center for Molecular Medicine in the Helmholtz Association, 13125 Berlin, Germany
[d] Charité – Universitätsmedizin Berlin, corporate member of Freie Universität Berlin, Humboldt-Universität zu Berlin, and Berlin Institute of Health, NeuroCure Clinical Research Center, 10117 Berlin, Germany.
[e] Charité – Universitätsmed≥≥izin Berlin, corporate member of Freie Universität Berlin, Humboldt-Universität zu Berlin, and Berlin Institute of Health, Department of Neurology and Experimental Neurology, 10117 Berlin, Germany
[f] Charité – Universitätsmedizin Berlin, corporate member of Freie Universität Berlin, Humboldt-Universität zu Berlin, and Berlin Institute of Health, Department of Psychiatry and Psychotherapy, 12203 Berlin, Germany
[g] Charité – Universitätsmedizin Berlin, corporate member of Freie Universität Berlin, Humboldt-Universität zu Berlin, and Berlin Institute of Health, Department of Endocrinology and Metabolism, 10117 Berlin, Germany
[h] Charité – Universitätsmedizin Berlin, corporate member of Freie Universität Berlin, Humboldt-Universität zu Berlin, and Berlin Institute of Health, Max Rubner Center for Cardiovascular-Metabolic-Renal Research, 10117 Berlin, Germany
[i] Berlin Institute of Health, 10117 Berlin, Germany
[j] Charité – Universitätsmedizin Berlin, corporate member of Freie Universität Berlin, Humboldt-Universität zu Berlin, and Berlin Institute of Health, DZHK (German Centre for Cardiovascular Research), Partner Site Berlin, 13347 Berlin, Germany
[k] Melbourne School of Psychological Sciences, Faculty of Medicine, Dentistry and Health Sciences, University of Melbourne, Redmond Barry Building #817, Parkville, Victoria, 3010, Australia
[l] Charité – Universitätsmedizin Berlin, corporate member of Freie Universität Berlin, Humboldt-Universität zu Berlin, and Berlin Institute of Health, Department of Psychosomatic Medicine, 10117 Berlin, Germany
[m] Institute of Neuroimmunology and Multiple Sclerosis (INIMS), Center for Molecular Neurobiology Hamburg, Universitätsklinikum Hamburg-Eppendorf, 20251 Hamburg, Germany

SUPPLEMENTARY MATERIAL

Keywords: Multiple sclerosis, obesity, psychological stress, functional connectivity, glucocorticoid functioning

Acknowledgments and Funding: This work was supported by the German Research Foundation (WE 5967/2-1 and WE 5967/2-2 to MW, GO 1357/5-1 and GO 1357/5-2 to SMG, Exc 257 to FP). Our funding sources did not influence the study design, the collection, analysis and interpretation of data, the writing of the report or the decision to submit the article for publication.

*These authors contributed equally.

§Corresponding author. E-mail address: weygandtmartin@gmail.com

Methods

Heart rate computation

The standard pulse oxymeter of the Physiological Monitoring Unit that came with the MRI scanner was used to determine the heart rate during the rest and stress fMRI measurements. The photoplethysmograph detector was mounted to the participants' toes as the experimental paradigm required them to manually operate button boxes. The quality of heart rate signals obtained from participants' toes is comparable to signals obtained from their fingertips (Hinkelbein et al. 2005). One heart rate parameter was calculated for each participant and each of the two conditions. In particular, in the first study project one (e.g., Weygandt et al., 2016), we removed pulse oximeter raw signal artifacts that would have resulted in a heart rate acceleration of ≥ 133% or a deceleration of ≤ 75% in a first step. The remaining data from the (final) 8 min of both conditions were then utilized to compute the average heart rate for a given participant and condition as indicator of heart rate of a given condition and participant in a second. In the second study project (e.g., Brasanac et al., 2022), we first computed a Fourier analysis to calculate the amplitude spectrum of heart rate time series based on the raw pulse signals of the (final) 8 min of both conditions separately for each condition and participant. To limit the fit to the physiologically meaningful frequency spectrum, frequencies below 30 Hz and above 150 Hz were eliminated. Amplitudes in two frequency windows (47.6 to 48.4 Hz, and 95.6 to 96.4 Hz) were also eliminated due to a technical artifact produced in these frequency ranges by the pulse oximeter. In a second step, we fitted a unimodal gaussian to the calculated amplitude spectrum for both periods. We then used the frequency with the largest fitted amplitude as the indicator of heart rate of a given condition and participant.

MRI acquisition

All brain scans were performed with a 3 Tesla whole-body tomograph (Magnetom Trio, Siemens, Erlangen, Germany) using a standard head coil with twelve channels.

Anatomical scans

In the first study project, two anatomical MR sequences were acquired. In particular, a T1-weighted sagittal 3-D-magnetization prepared rapid gradient echo (MP-RAGE) sequence (176 slices; slice thickness 1.3 mm; in-plane voxel resolution 1.5 · 1.5 mm^2; TR = 1720ms; TE = 2.34ms; FA = 9°; FOV = 192 · 192 mm^2; matrix size = 128 × 128; duration 1 min and 43 sec) and a sagittal T2-weighted (T2w) sequence to facilitate manual lesion mapping (176 slices; 1 mm isotropic voxels; TR = 5000 ms; TE = 502 ms; FA = 120°; FOV = 256 · 256 mm^2; matrix size = 256 · 256; 5 min and 52 sec duration) was used. In the second project, we used a T1-weighted sagittal 3D MP-RAGE echo sequence (176 slices; 1 mm isotropic voxels; TR = 1900 ms; TE = 3.03 ms; FA = 9°; FOV = 256 · 256 mm^2; matrix size = 256 × 256; 4 min 26 sec duration) as well as a sagittal T2-weighted FLAIR sequence (176 slices; 1 mm isotropic voxels; TR = 6000 ms; TE = 388 ms; TI = 2100 ms; FA = 120°; FOV = 256 · 256 mm^2; matrix size = 256 · 256; 7 min 44 sec duration).

Functional scans

In both study projects, perfusion brain images were acquired using a pseudo-continuous ASL Echo-Planar Imaging (EPI) sequence (Wang et al., 2005). This sequence comprised 22 ascending transversal slices and covered the whole brain (slice thickness 5.75 mm [including 15% inter-slice gap]; in-plane voxel resolution 3 · 3 mm^2; TR = 4000 ms; TE = 19ms; FA = 90°; FOV = 192 · 192 mm^2; matrix size = 64 · 64; label duration 1.5 sec, post-label delay 1.2 s; phase-encoding direction anterior to posterior). Moreover, we acquired two spin-echo EPI reference volumes with opposing phase encoding directions (anterior to posterior, posterior to anterior) in advance to the rest and the stress ASL measurements with matching readout and geometry in order to facilitate a distortion correction of ASL images.

MRI preprocessing

Anatomical scans

First, experienced raters conducted a manual mapping of localized lesions based on the T2 or FLAIR scans. A neuroradiologist oversaw these procedures. Next, the T2 or FLAIR scan of a given participant was co-registered to this participant's T1-weighted MP-RAGE scan. Afterwards, we determined voxel-wise tissue probability maps for GM, white matter (WM) and cerebro-spinal fluid (CSF) by applying the combined spatial normalization and segmentation algorithm of SPM12 to the T1-weighted MP-RAGE scans. Voxel locations included in the co-registered lesion masks were discarded in this combined normalization and segmentation procedure, which finally generated tissue probability maps for each of the three tissues. These ('modulated') tissue probability maps were adjusted for impacts of local deformations applied during spatial normalization and created in the anatomical standard space defined by the MNI. The transformation parameters determined in this procedure for mapping the T1-weighted images to the MNI space were also used to map the lesion masks coregistered to the space of the raw T1-weighted scans to the MNI space.

Afterwards, we used the modulated tissue probability maps to compute the whole-brain GM fraction for each patient. In particular, for each voxel, we identified the tissue with the largest modulated tissue probability in the given participant. We then assigned this voxel to the tissue identified except if its localization was within lesioned tissue as indicated by the MNI-space lesion mask. The GM tissue fraction was then calculated as the total number of GM voxels divided by the total number of intracranial voxels. Similarly, the lesion volume for each patient was computed by counting the number of lesion voxels within the lesion masks mapped to MNI space and then multiplying this count by the volume of voxels within this space, which corresponded to $3 \cdot 3 \cdot 3$ mm^3.

Similarly, group-masks for the three tissues (required in the analyses of functional MRI scans) were determined by determining the tissue with the largest modulated tissue probability across all participants per voxel and assigning this voxel to this tissue. In order to account for partial voluming effects, we deleted voxel coordinates from GM, WM, and CSF group masks that were directly located in lesioned tissue in at least one participant or in the

six neighboring voxels (i.e., those six voxels that had a Euclidean distance of exactly one voxel to a lesion voxel of a participant; cf. Weygandt et al., 2011).

Functional scans

Preprocessing of ASL scans was performed with the SPM12 ACID (Ruthotto et al., 2008) and ASLtbx (Wang et al., 2008) toolboxes.

Quality assurance step for functional scans using the Framewise Displacement metric

The framewise displacement (FWD) measure, a well-known technique proposed by Power et al. (2014) that assesses participants' fMRI head motion parameters (here determined during preprocessing of functional ASL scans), was used to perform an fMRI image data quality assurance step. Specifically, for each condition (i.e., rest and stress) and each of the 60 participants available (20 from Weygandt et al., 2016, 40 from Brasanac et al., 2022), first one average motion-based image quality marker ("FWD score") was calculated based on the head motion parameters determined during preprocessing of ASL scans. In the next step, we looked for outliers among the FWD scores across the pooled sample of 60 patients for each condition separately. In particular, an FWD score was deemed an outlier if more extreme than the first (third) quartile minus (plus) 1.5 times the inter-quartile range of the FWD scores computed for this condition. Only participants who had non-outlier FWD scores in both conditions passed the procedure. This was the case for all 20 participants taken from Weygandt et al. (2016), and for 37 from Brasanac et al. (2022).

Regional neural stress reactivity within patients

In order to determine the regional neural stress reactivity, we first corrected the rCBF time series of each voxel, condition, and participant for head motion (Wang et al., 2012; Wang et al., 2008) and global WM and CSF signals (Arnemann et al., 2015; Wang et al., 2012). Head motion parameters were computed by ASLtbx, the average signal across all voxels contained

in the group-specific WM and CSF masks were computed for each participant as global WM and CSF signals.

Next, we determined an rCBF timeseries for each condition, participant, and region included in the Neuromorphometrics brain atlas (http://Neuromorphometrics.com) averaged across timeseries of all voxels in that region if the given voxel was included in the GM group mask and contained non-zero rCBF. An atlas region was excluded from all fMRI analyses if not containing at least a single voxel meeting these criteria across all participants. From the 122 regions in the atlas, only three, i.e., left and right pallidum as well as cerebellar vermal lobules VIII-X, were not included. Exclusion of these regions followed from the facts that (i) the GM contrast in the pallidum is relatively weak in MP-RAGE scans (Droby et al., 2021), (ii) MS lesions occur frequently close to pallidum, (iii) the location of cerebellar vermal lobules VIII-X was close to the inferior boundary of the ASL measurement region (i.e., its Field of View), (iv) we excluded regions already if they did not fulfill the abovementioned criteria in a single participant.

To finally compute measures of regional stress reactivity, we concatenated both conditions' regional time series in each participant and region and used linear regression to determine regional activity differences between the stress and the rest condition. The concatenated time series served as dependent variable and a boxcar regressor coding zeros for the 60 rCBF data points of the rest condition and ones for the 60 rCBF data points of the last 8 min of the stress condition served as predictor (e.g., Wang et al., 2012; Wang et al., 2008). This procedure was carried out for each person and region included in the analysis. The region-by-region regression coefficients obtained were entered into main analysis 2 (as well as in supplementary analysis 2) as regional stress reactivity indicators.

Gene expression in T cellular glucocorticoid pathway

Isolation of Peripheral Blood Mononuclear Cells

A venous blood sample (about 70ml) was taken from participants at the morning of the clinical examination and processed within two hours. Particularly, in accordance with standard operating procedures (Hasselmann et al., 2018), peripheral blood mononuclear

cells (PBMCs) were isolated with density gradient centrifugation. Specifically, blood was diluted first in phosphate-buffered saline (PBS) (1:1). Afterwards, 35ml of the diluted blood were layered carefully in a 50ml conical tube on top of 15ml of Biocoll medium (Biochrom, Berlin, Germany). The tubes were centrifuged at 870 × g (brakes off) for 30 min. After the mononuclear cell layer was harvested from the interphase, cells were washed twice in cold PBS for 10 min each. In order to prepare the PBMCs for cryopreservation, they were pelleted and then resuspended in RPMI-1640 (Gibco, ThermoFisher Scientific, Berlin, Germany), which was supplemented with 25% heat-inactivated fetal bovine serum (FBS; Biochrom, Berlin, Germany) and 10% dimethylsulfoxide (Applichem GmbH, Darmstadt, Germany). Next, cells were counted and then diluted to a concentration of 10 million cells per milliliter in 1.5ml tubes (Eppendorf, Hamburg, Germany), and placed in a freezing container (Sigma-Aldrich, St. Louis, USA) for overnight cooling at -80 °C. Frozen tubes were moved to a long-term liquid nitrogen storage tank (-196 °C) the following day where they remained until further examination.

Cell sorting, RNA isolation, cDNA synthesis, and real-time PCR

Magnetic-activated cell sorting (MACS), which divides cells based on surface antigens, was used to separate $CD4^+$ and $CD8^+$ T cell subsets. After thawing in a warm water bath (37 °C) for one to 2 min, tubes containing PBMCs were washed for 6 min at 250 × g in warmed RPMI-1640 medium containing 10% FBS. Following the manufacturer's recommendations, cell sorting was then carried out using CD4 and CD8 MicroBeads (Miltenyi Biotec, Bergisch Gladbach, Germany). 20µl of CD4 MicroBeads (Miltenyi Biotec, Bergisch Gladbach, Germany) and 80ml of MACS buffer (phosphate-buffered saline, 0.5% BSA, 2 mM EDTA) per 10 million cells were added, and the mixture was incubated for 15 min at 4°C in the dark. After washing with MACS buffer for 5 min at 350 × g (4 °C) cells were resuspended in 500µl MACS buffer. Next, MACS LS columns (Miltenyi Biotec, Bergisch Gladbach, Germany) were used to isolate $CD4^+$ T cells. The $CD4^-$ negative percentage was then used for sorting $CD8^+$ T cells in the following phase, adhering to a similar protocol: CD8 MicroBeads (Miltenyi Biotec, Bergisch Gladbach, Germany) were used to label the cells. The cells were then incubated on the MACS MS columns, separated, and ultimately resuspended in 500µl of MACS buffer. Using flow

cytometry (FACSCanto II, BD Biosciences, New Jersey, USA), cell fraction purity was checked. The purity coefficients were 91.67% + 6.74 SD (0.89 SEM) for $CD4^+$ T cells and 95.15% + 5.73 SD (0.76 SEM) for $CD8^+$ T cells. Following the recommendations of the manufacturer, total RNA was extracted from $CD4^+$ and $CD8^+$ T cell fractions with the Qiagen RNeasy Plus Mini Kit (Qiagen, Hilden, Germany). A NanoDrop spectrophotometer (NanoDrop 2000c, Thermo Fisher Scientific, Berlin, Germany) was used to evaluate their purity and concentration. Complementary DNA (cDNA) was transcribed from RNA in the next step in accordance with the manufacturer's instructions using Thermo Fisher Scientific's RevertAid H Minus First Strand cDNA Synthesis Kit and kept at -20 °C. TaqMan Gene Expression Assays (Thermo Fisher Scientific, Berlin, Germany) were employed to amplify cDNA with a StepOne real-time PCR System for GR (Hs00353740 m1), FKBP5 (Hs01561006 m1), FKBP4 (Hs00427038 g1), and GILZ (Hs00608272 m1). Triplicates were used to run real-time PCR experiments. Two housekeeping genes, TATA Box Binding Protein (TBP; Hs00427620 m1) and Importin 8 (IPO8; Hs00183533 m1), were used to standardize gene expression. These housekeeping genes were chosen as reliable gene references for gene expression analyses in human T cells (Ledderose et al., 2011). By subtracting the geometric mean of housekeeping genes from the mean CT values of a given gene of interest, delta cycle threshold (ΔCT) values were computed as markers of gene expression within the glucocorticoid pathway. These ΔCT values were entered in the third and fourth main analyses for evaluation.

Statistical analysis

Analysis 4: BMI-related glucocorticoid and neural processing markers

Explanation of the number of tests conducted

Sixty-two (i.e., $2 \cdot [2 \cdot 16 - 1] = 62$) tests were conducted in main analysis 4. Specifically, 2 T cell GC sensitivity markers were significantly related to BMI and thus evaluated per family of tests, 2 regions showed a FC significantly linked to BMI during rest or stress respectively and thus served as FC seed region, and each of these 2 seed regions had 16 (i.e., 17 – 1) FC target regions. However, as one pair among the $2 \cdot 16$ pairs of stress-reactive seed-target regions

was redundant, it did not contribute to the number of tests and was thus subtracted (→ 2 · 16 - 1; see Fig. 6a).

Supplementary analysis 1: Psychological and peripheral stress responses

We used linear mixed models to test perceived stress (based on self-report data acquired in both rating stages included in the analyses and available for all 57 PwMS) and peripheral stress responses (i.e., differences in the heart rate between the rest stage and the final 8 min of the stress stage; available for 51 PwMS). The CNI were the same as in main analysis 2. Again, we applied permutation testing for inference.

Supplementary Analysis 2: BMI and brain activity of stress-responsive regions

Here, we repeated main analysis 2 but instead of regressing the participants FC on their BMI, we modeled the regional stress response activity parameters (i.e., the coefficients described in section 'Regional neural stress reactivity within patients' above) based on their BMI. CNI were the same as in main analysis 2. Again, we applied a significance threshold corrected for multiple testing of $\alpha_{FWE} = 0.05$. However, other than in main analysis 2, the equivalent of this FWE-corrected threshold on the single test level was $0.05/17 = 0.0029$ as the number of tests equaled to the number of significant stress responsive regions (i.e., 17) and not the number of pairs of significant stress responsive regions (i.e., 136).

Supplementary analysis 3: Impact of patients' sex on DVs tested in main analyses 1 – 4

Given the well-established sex differences in autoimmune disorders, including MS (Gold et al., 2019), we investigated whether patients' sex was related to the DVs tested across main analyses 1 – 4. Importantly, because patients' sex was included in all regression analyses computed throughout these analyses as CNI (and a putative impact of sex on the associations primarily tested in these analyses was thus statistically controlled), this potential relation was automatically determined by the regression models computed for the primary aims of main analyses 1 - 4 as byproduct. Consequently, the statistical parameters reported for sex

and the methodology employed to assess the relationship between sex and the DVs were identical to those reported for the CI in main analyses 1 – 4.

Supplementary analysis 4: Differences between BMI-derived body mass groups

In main analyses 1 – 4, we tested associations between the continuous BMI variable and DVs using linear robust regression analyses applied to the data of all patients. Although this approach has serious advantages over analyzing the impact of body mass on variables of interest by contrasting groups characterizing individuals' body mass in a categorial fashion (i.e., as obese, underweight, etc.) in case of the present study (see the Discussion in the main text), it might be unable to discover non-linear associations between a variable and body mass. For example, it might miss if underweight and obese individuals have high values in a variable and normal-weight and overweight persons have low ones. Other than the linear regression analyses in the main text, however, ANCOVA is able to detect such non-linear associations. For this reason, and due to the popularity of the categorial body mass labels, we conduct complementary ANCOVA testing differences between body mass groups (i.e., obesity [BMI ≥ 30], overweight [25 ≥ BMI > 30], etc.) in the DV tested in the main analyses in this supplementary analysis.

Methodologically, this was achieved by generating a regression model including dummy variables coding for group membership in a binary fashion (instead of the single continuous BMI regressor) and the same CNI as in the corresponding main analyses. Determined by ANCOVA, F-values are reported as test statistic. Again, robust regression was used to determine the model parameters and permutation testing (10,000 permutations of the group vector [coding 1 for underweight, 2 for normal weight, 3 for overweight, and 4 for obesity] used for setting up the dummy variables) for inference. Also, the significance thresholds employed were the same as in the main analyses. Partial Eta^2 (η_p^2) is reported as measure of effect size. According to Cohen (1988), $\eta_p^2 \geq 0.01$ corresponds to a small, $\eta_p^2 \geq 0.06$ to a medium, and $\eta_p^2 \geq 0.14$ to a large effect.

Results

Main analysis 1: BMI and MS activity and severity

Properties of f^2 based on robust coefficients of determination

In this analysis, small negative values for f^2 were obtained for two MS severity parameters (i.e., lesion load: $t = 0.26$, $p = 0.792$, $= p_{FWE} > 0.999$, $f^2 = -0.00$ and GM fraction: $t = 0.24$, $p = 0.812 = p_{FWE} > 0.999$, $f^2 = -0.01$). These small negative f^2 values can result from specifics of f^2 and the use of robust coefficients of determination R^2_{full} and R^2_{base} for its computation ($f^2 = [R^2_{full} - R^2_{base}] / [1 - R^2_{full}]$; cf. Renaud et al., 2010), which is a necessary step when employing robust regression methods because standard (i.e., non-robust) coefficients of determination do not reflect the impact of the robust algorithms on the regression model. In particular, the difference in the variance explained in the dependent variable between the base model and the full model (i.e., between R^2_{full} and R^2_{base}) must only rely on the presence of the variable for which the effect size should be determined in the full model and the absence of this variable in the base model when estimating f^2. As no parameters have to be optimized in ordinary (i.e., non-robust) regression besides the regression coefficients, this prerequisite holds within this regression method. In robust regression, however, this is different as it additionally scales individual observations by computing observation weights to achieve a more robust regression solution in case of outliers. Consequently, the difference in the variance explained in the dependent variable between R^2_{full} and R^2_{base} could not only depend on the presence/absence of the variable in question but also in differences between the observation weights when these weights would be computed individually for the base and the full model. To address this issue, one can (and we did) use the observation weights computed for the full model for calculating not only R^2_{full} but also R^2_{base}. Under these circumstances, small negative values for f^2 can result.

Supplementary analysis 1: Psychological and peripheral stress responses

The task induced a pronounced psychological ($t = 9.31$, $p < 10^{-4}$, $f^2 = 0.99$) and peripheral ($t = 6.05$, $p < 10^{-4}$, $f^2 = 0.71$) stress response. Fig. S1 provides further details.

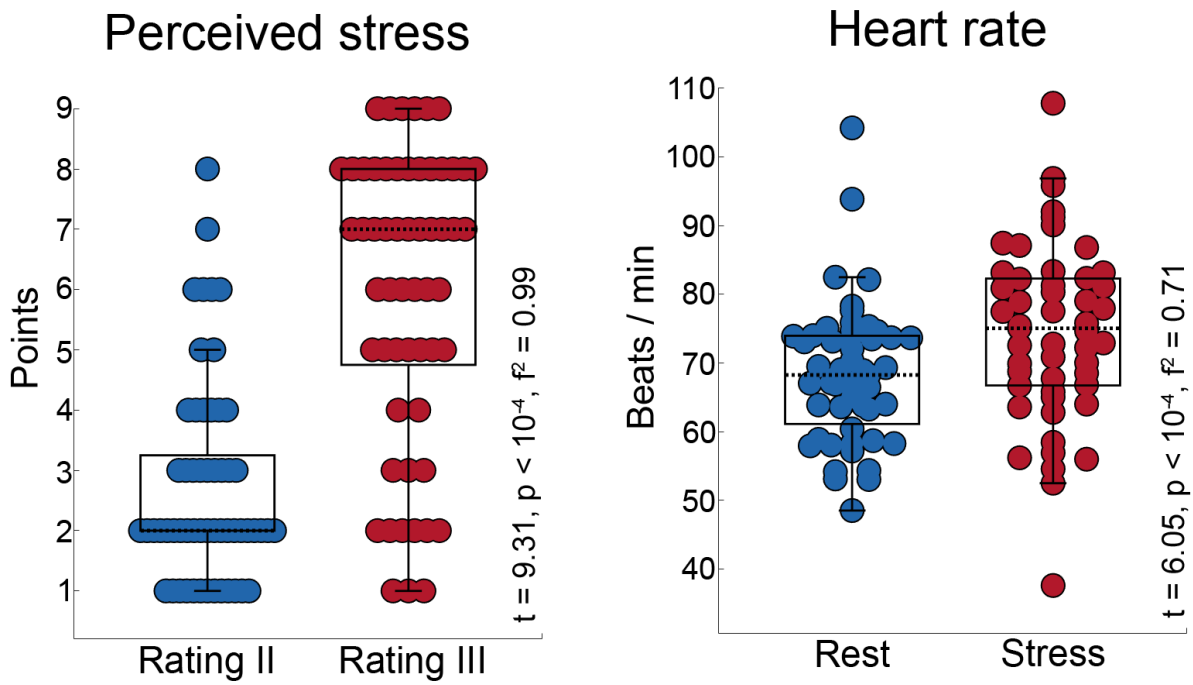

Figure S1 depicts the stress response induced by the task in terms of psychological stress (ratings of perceived stress) on the left and in terms of heart rate accelerations on the right. The lower, center, and upper edges of the black boxes depict the first, second (i.e., median), and third quartile of the distribution of parameters.

Supplementary Analysis 2: BMI and brain activity of stress-responsive regions

We found for none of the 17 regions a significant association between BMI and stress-response activity. Specifically, for the most extreme t-statistic obtained in this analysis (i.e., for the association between BMI and right anterior insula activity differences), the type I error rate was p = 0.01, which is much larger than the required p-value of 0.0029. Fig. S2 provides an illustration.

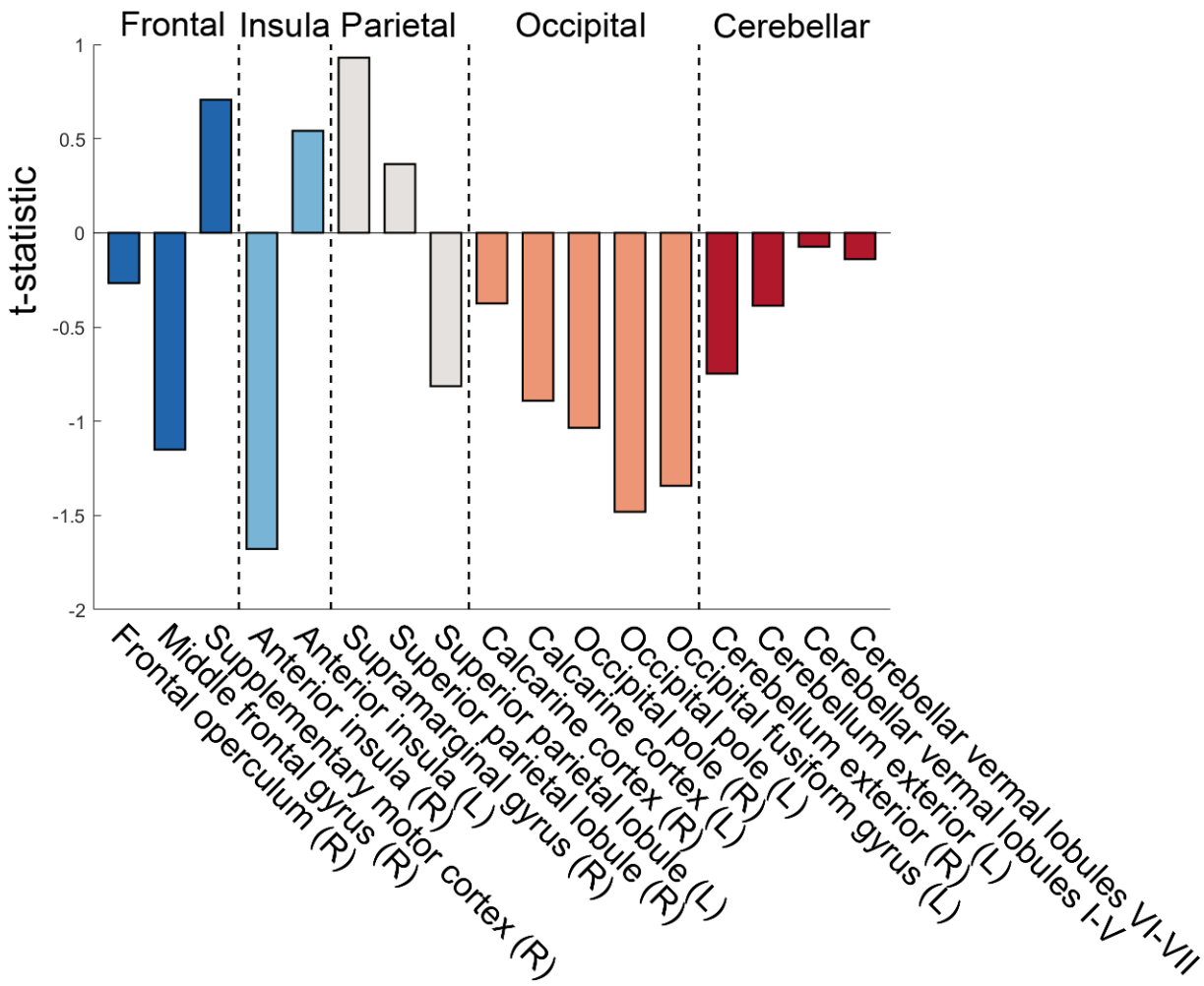

Figure S2 illustrates the associations between the BMI and the regional stress response activity of stress-reactive regions.

Supplementary analysis 3: Impact of patients' sex on DVs tested in main analyses 1 – 4

The impact of patients' sex on the DVs tested across main analyses 1 – 4 was very small. In particular, among all the variables tested, sex was related to a single variable (and only at an $\alpha_{FWE} = 0.1$ level, which would not have been reported for the CI in main analyses 1 – 4): patients' GM fraction. Specifically, men tended to have a lower GM fraction than women. Figure S3 illustrates these results.

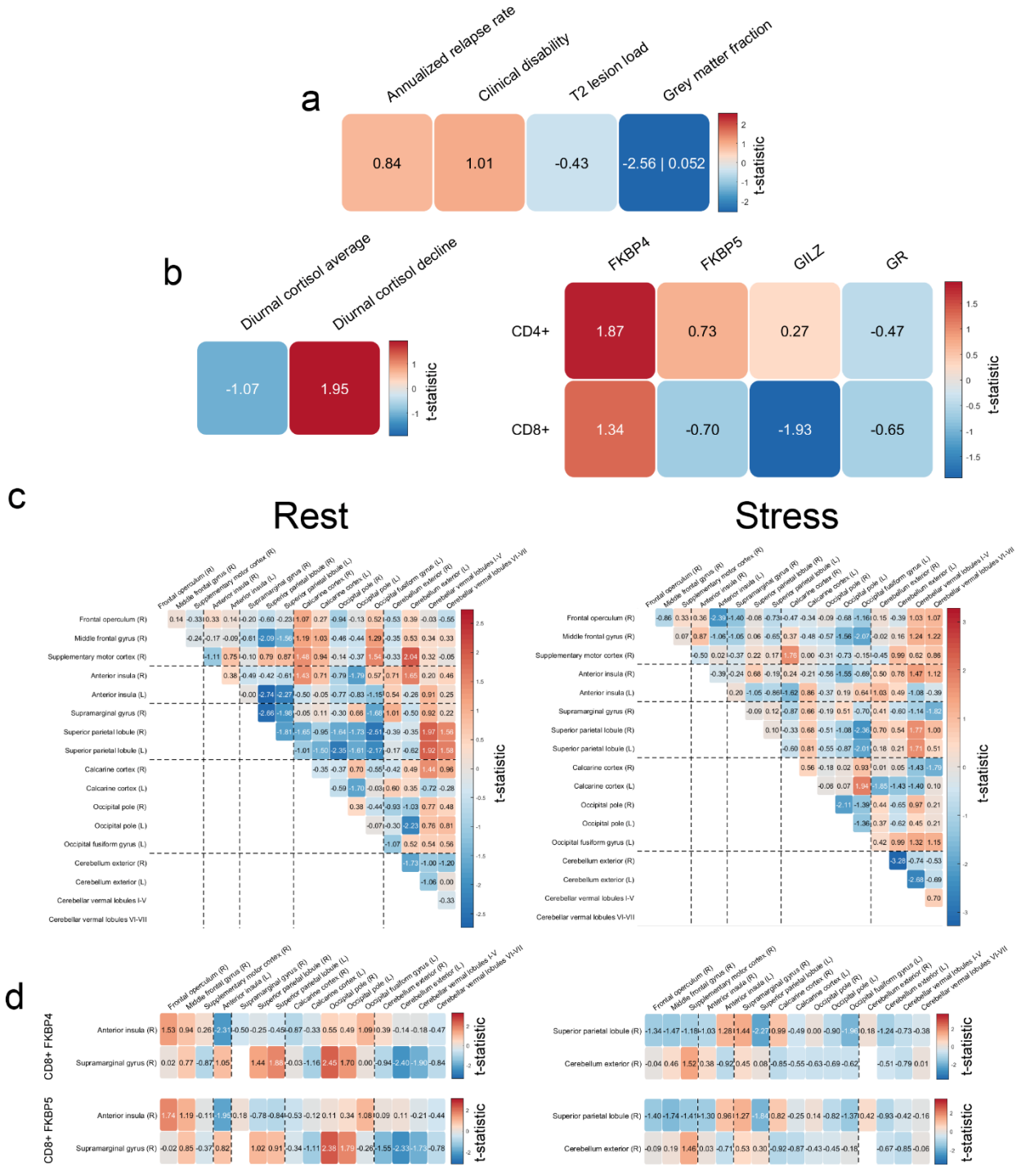

Figure S3 reports the t-statistic for sex obtained by the same linear regression models as used for determining the effects tested in main analyses 1 - 4. In particular, Figure S3a / b / c /d show the t-statistics for sex obtained from the models computed for main analysis 1 / 2 / 3 / 4. In the only case where a significant result was obtained (however, at an $\alpha_{FWE} = 0.1$ level only), for the association between patients' sex and the whole-brain GM fraction, we additionally report p_{FWE}.

Supplementary analysis 4: Differences between BMI-derived body mass groups

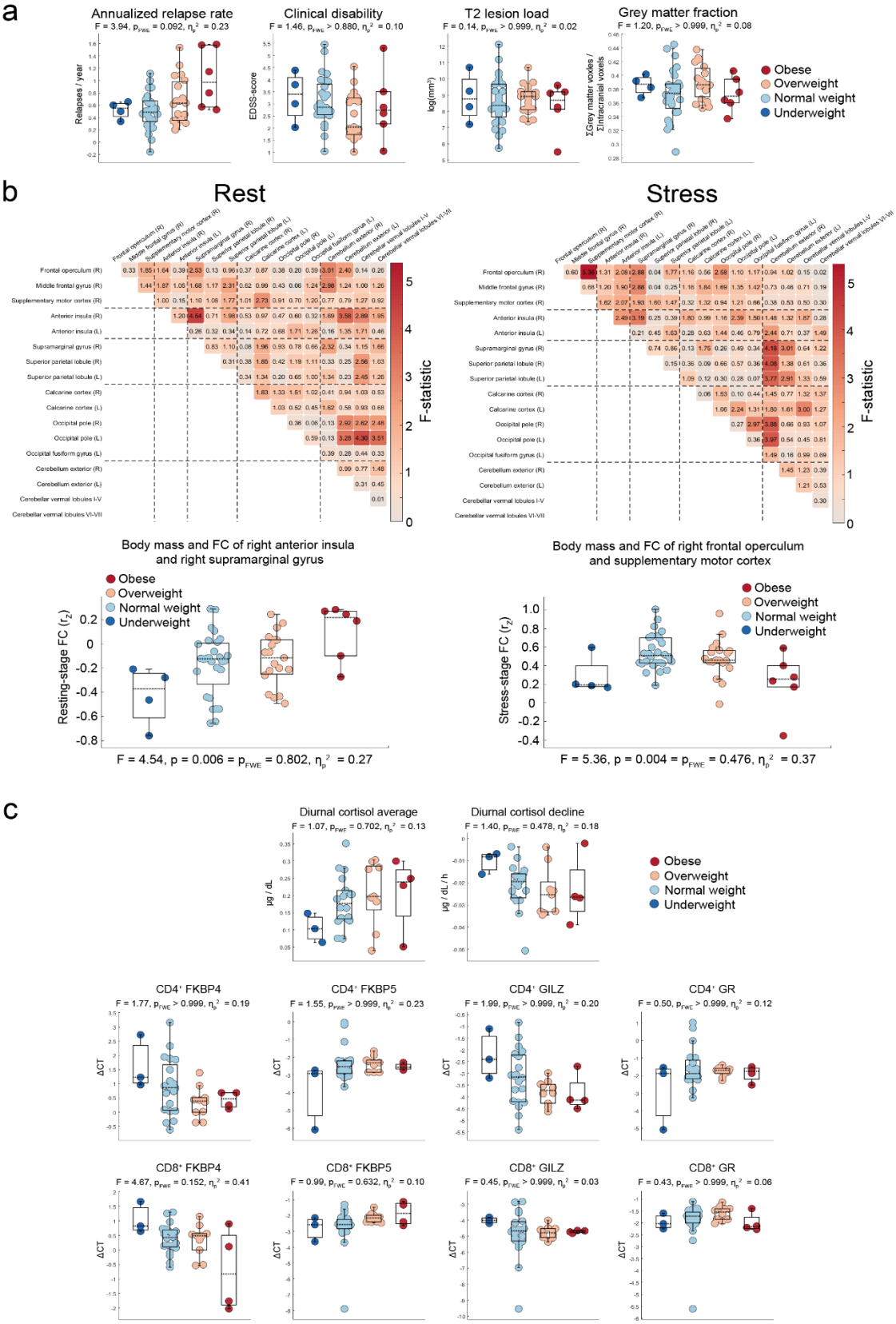

Figure S4 shows the results obtained for testing the effects evaluated in main analyses 1 to 3 by applying one-factorial ANCOVA of body mass categories instead of regression analyses evaluating the continuous BMI measure. In particular, Figure S4a / b / c shows the results obtained for repeating tests in a categorial fashion that were addressed in in a continuous fashion in main analysis 1 / 2 / 3. Please note, that tests conducted in main analysis 4 were not repeated using ANCOVA since main analysis 4 was a post-hoc analysis relying on the significance of results obtained in main analyses 2 and 3 and their ANCOVA counterparts failed to reveal significant results. Across all boxplot graphs depicted in S4a / b / c, the DVs plotted on the y-axis were corrected for CNI.

Although a visual comparison of Figures 2 – 4 in the main text with Figure S4 shows that the overall pattern of results obtained for body mass groups is comparable to that obtained for continuous BMI values (when considering that the F-distribution is asymmetric and ranges from 0 to $+\infty$ whereas the t-distribution is symmetric and ranges from $-\infty$ to $+\infty$), it is noteworthy that the p-values obtained through ANCOVA are systematically higher than those obtained for continuous BMI values. More specifically, not a single ANCOVA obtained significant results on an $\alpha_{FWE} = 0.05$ level.

References

Arnemann KL, Chen AJW, Novakovic-Agopian T, Gratton C, Nomura EM, D'Esposito M. Functional brain network modularity predicts response to cognitive training after brain injury. Neurology. 2015;84:1568-74.

Brasanac J, Hetzer S, Asseyer S, Kuchling J, Bellmann-Strobl J, Ritter K, Gamradt S, Scheel M, Haynes JD, Brandt AU, Paul F*, Gold SM*, Weygandt M*,§. Central stress processing, T cell responsivity to stress hormones, and disease severity in multiple sclerosis. Brain Commun. 2022. 4: fcac086.

Cohen J. Statistical Power Analysis for the Behavioral Sciences. 1988; 2nd ed., Lawrence Erlbaum Associates: Hillsdale.

Droby A, Thaler A, Giladi N, Hutchison RM, Mirelman A, Ben Bashat D, et al. (2021) Whole brain and deep gray matter structure segmentation: Quantitative comparison between MPRAGE and MP2RAGE sequences. PLoS ONE16(8): e0254597Gold SM, Willing A, Leypoldt F, Paul F, Friese MA. Sex differences in autoimmune disorders of the central nervous system. Semin Immunopathol. (2019) 41:177–88.

Gold SM, Willing A, Leypoldt F, Paul F, Friese MA. Sex differences in autoimmune disorders of the central nervous system. Semin Immunopathol. 2019; 41: 177-188. doi: 10.1007/s00281-018-0723-8.

Hasselmann H, Gamradt S, Taenzer A, et al. Pro-inflammatory Monocyte Phenotype and Cell-Specific Steroid Signaling Alterations in Unmedicated Patients with Major Depressive Disorder. Front Immunol. 2018;92693.

Hinkelbein J, Hose D, Fiedler F. Comparison of three different sensor sites for pulse oximetry. International Journal of Intensive Care. 2005; 1 – 5.

Ledderose, C., Heyn, J., Limbeck, E. and Kreth, S. Selection of reliable reference genes for quantitative real-time PCR in human T cells and neutrophils. BMC Research Notes. 2011;4:427.Power JD, Mitra A, Laumann TO, Snyder AZ, Schlaggar BL, Petersen SE (2014) Methods to detect, characterize, and remove motion artifact in resting state fMRI. NeuroImage 84:320-41.

Power JD, Mitra A, Laumann TO, Snyder AZ, Schlaggar BL, Petersen SE. Methods to detect, characterize, and remove motion artifact in resting state fMRI. NeuroImage. 2014; 84:320-41.

Renaud O, Victoria-Feser MP. A Robust Coefficient of Determination for Regression. J Stat Plan Inference. 2010; 1852-1862.

Ruthotto L, Kugel H, Olesch J, Fischer B, Modersitzki J, Burger M. Diffeomorphic Susceptibility Artefact Correction of Diffusion-Weighted Magnetic Resonance Images. Phys Med Biol. 2012; 57: 5715-31.

Wang Z, Aguirre GK, Rao H, Wang J, Fernandez-Seara MA, Childress AR. Empirical optimization of ASL data analysis using an ASL data processing toolbox: ASLtbx. Magn Reson Imag. 2008; 26 (2): 261 – 9.

Wang Z. Improving cerebral blood flow quantification for arterial spin labeled perfusion MRI by removing residual motion artifacts and global signal fluctuations. Magnetic Resonance Imaging 30 (2012) 1409-1415.

Wang Z, et al. (2008) Empirical optimization of ASL data analysis using an ASL data processing toolbox: ASLtbx. Magn Reson Imag 26 (2): 261 - 9.

Wang J, Rao H, Wetmore GS, Furlan PM, Korczykowski M, Dinges DF, Detre JA (2005) Perfusion functional MRI reveals cerebral blood flow pattern under psychological stress. Proc Natl Acad Sci U S A 102:17804-9.

Weygandt M Meyer-Arndt L Behrens J, Wakonig K, Bellmann-Strobl J, Ritter K, Scheel M, Brandt AU, Labadie C, Hetzer S, Gold SM, Paul F, Haynes JD (2016). Stress-induced brain activity, brain atrophy, and clinical disability in Multiple Sclerosis. Proceedings of the National Academy of Science USA. 113: 13444–13449.

Weygandt M, et al. (2011) MRI Pattern Recognition in Multiple Sclerosis Normal-Appearing Brain Areas. PLoS ONE 6: e21138. doi: 10.1371/journal.pone.0021138.